

MIIND : A Model-Agnostic Simulator of Neural Populations

Hugh Osborne¹, Yi Ming Lai², Mikkel Elle Lepperød³, David Sichau⁴, Lukas Deutz¹ and Marc de Kamps^{1,*}

¹ Institute for Artificial Intelligence and Biological Computation, School of Computing, University of Leeds, Leeds, United Kingdom

² School of Medicine, University of Nottingham, Nottingham, United Kingdom

³ Centre for Integrative Neuroplasticity, University of Oslo, Oslo, Norway

⁴ Department of Computer Science, ETH Zurich, Zurich, Switzerland

Correspondence*:

Marc de Kamps

M.deKamps@leeds.ac.uk

2 ABSTRACT

3 MIIND is a software platform for easily and efficiently simulating the behaviour of interacting
4 populations of point neurons governed by any 1D or 2D dynamical system. The simulator is
5 entirely agnostic to the underlying neuron model of each population and provides an intuitive
6 method for controlling the amount of noise which can significantly affect the overall behaviour. A
7 network of populations can be set up quickly and easily using MIIND's XML-style simulation file
8 format describing simulation parameters such as how populations interact, transmission delays,
9 post-synaptic potentials, and what output to record. During simulation, a visual display of each
10 population's state is provided for immediate feedback of the behaviour and population activity
11 can be output to a file or passed to a Python script for further processing. The Python support
12 also means that MIIND can be integrated into other software such as The Virtual Brain. MIIND's
13 population density technique is a geometric and visual method for describing the activity of each
14 neuron population which encourages a deep consideration of the dynamics of the neuron model
15 and provides insight into how the behaviour of each population is affected by the behaviour of its
16 neighbours in the network. For 1D neuron models, MIIND performs far better than direct simulation
17 solutions for large populations. For 2D models, performance comparison is more nuanced but the
18 population density approach still confers certain advantages over direct simulation. MIIND can be
19 used to build neural systems that bridge the scales between an individual neuron model and a
20 population network. This allows researchers to maintain a plausible path back from mesoscopic to
21 microscopic scales while minimising the complexity of managing large numbers of interconnected
22 neurons. In this paper, we introduce the MIIND system, its usage, and provide implementation
23 details where appropriate.

24 **Keywords:** Simulator, Neural Population, Population Density, Software, Python, Dynamical Systems, Network, GPU

1 INTRODUCTION

25 1.1 Population-Level Modeling

26 Structures in the brain at various scales can be approximated by simple neural population networks
27 based on commonly observed neural connections. There are a great number of techniques to simulate the
28 behaviour of neural populations with varying degrees of granularity and computational efficiency. At the
29 highest detail, individual neurons can be modelled with multiple compartments, transport mechanisms, and
30 other biophysical attributes. Simulators such as GENESIS (Wilson et al., 1988; Bower and Beeman, 2012)
31 and NEURON (Hines and Carnevale, 2001) have been used for investigations of the cerebellar microcircuit
32 (D’Angelo et al., 2016) and a thalamocortical network model (Traub et al., 2005). Techniques which
33 simulate the individual behaviour of point neurons such as in NEST (Gewaltig and Diesmann, 2007), or
34 the neuromorphic system SpiNNaker (Furber et al., 2014), allow neurons to be individually parameterised
35 and connections to be heterogeneous. This is particularly useful for analysing information transfer such as
36 edge detection in the visual cortex. They can also be used to analyse so called finite-size effects where
37 population behaviour only occurs as a result of a specific realisation of individual neuron behaviour. There
38 are, however, performance limitations on very large populations in terms of both computation speed and
39 memory requirements for storing the spike history of each neuron.
40

41 At a less granular level, rate-based techniques are a widely used practice of modeling neural activity with
42 a single variable, whose evolution is often described by first-order ordinary differential equations, which
43 goes back to Wilson and Cowan (1972). The Virtual Brain (TVB) uses these types of models to represent
44 activity of large regions (nodes) in whole brain networks to generate efficient simulations (Sanz Leon et al.,
45 2013; Jirsa et al., 2014). TVB demonstrates the benefits of a rate based approach with the Epileptor neural
46 population model yielding impressive clinical results (Proix et al., 2017). The Epileptor model is based
47 on the well known Hindmarsh-Rose neuron model (Hindmarsh and Rose, 1984). However, the behaviour
48 of this and other rate based models is defined at the population level instead of behaviour emerging from
49 a definition of the underlying neurons. Therefore, these models have less power to explain simulated
50 behaviours at the microscopic level.
51

52 Between these two extremes of granularity is a research area which bridges the scales by deriving
53 population level behaviour from the behaviour of the underlying neurons. So called population density
54 techniques (PDTs) have been used for many years (Knight, 1972; Knight et al., 1996; Omurtag et al., 2000)
55 to describe a population of neurons in terms of a probability density function. The transfer function of a
56 neuron model or even an experimental neural recording can be used to approximate the response from a
57 population using this technique (Wilson and Cowan, 1972; El Boustani and Destexhe, 2009; Carlu et al.,
58 2020). However, analytical solutions are often limited to regular spiking behaviour with constant or slowly
59 changing input. The software we present here, MIIND, provides a numerical solution for populations of
60 neurons with potentially complex behaviours (for example bursting) receiving rapidly changing noisy input
61 with arbitrary jump sizes. The noise is usually assumed to be shot noise, but can be non-Markovian (Lai and
62 de Kamps, 2017). It contains a number of features that make it particularly suitable for dynamical systems
63 representing neuronal dynamics, such as an adequate handling of boundary conditions that emerge from the
64 presence of thresholds and reset mechanisms, but is not restricted to neural systems. The dynamical systems
65 can be grouped in large networks, which can be seen as the model of a neural circuit at the population level.
66

67 The key idea behind MIIND is shown in Fig. 1A. Here, a population of neurons is simulated. In this case,
68 the neurons are defined by a conductance based leaky-integrate-and-fire neuron model with membrane
69 potential and state of the conductance as the two variables. The neuron's evolution through state space is
70 given by a two-dimensional dynamical system. The positions of individual neurons change in state space,
71 both under the influence of the neuron's endogenous dynamics as determined by the dynamical system and
72 of spike trains arriving from neurons in other populations, which cause rapid transitions in state space that
73 are modeled as instantaneous jumps. For the simulation techniques mentioned earlier involving a large
74 number of individual model neuron instances, a practice that we will refer to as Monte Carlo simulation,
75 the population can be represented as a cloud of points in state space. The approach in MIIND, known as
76 a population density technique (PDT) models the probability density of the cloud, shown in Fig. 1 as a
77 heat map, rather than the behaviour of individual neurons. The threshold and reset values of the underlying
78 neuron model are visible in the hard vertical edges of the density in Fig. 1A. In Fig. 1B, the same simulation
79 approach is used for a population of Fitzhugh-Nagumo neurons (FitzHugh, 1961; Nagumo et al., 1962).
80 The Fitzhugh-Nagumo model has no threshold-reset mechanism and so there are no vertical boundaries to
81 the density. As well as being informative in themselves, common population metrics such as average firing
82 rate and average membrane potential can be quickly calculated from these density functions.
83

84 1.2 The Case for Population Density Techniques

85 Why use this technique? Omurtag et al. (2000); Nykamp and Tranchina (2000); Kamps (2003); Iyer
86 et al. (2013) have demonstrated that PDTs are much faster than Monte Carlo simulation for 1D models;
87 De Kamps et al. (2019) have shown that while speed is comparable between 2D models and Monte Carlo,
88 memory usage is orders of magnitude lower because no spikes need to be buffered, which accounts for
89 significant memory use in large-scale simulations. In practice, this may make the difference between
90 running a simulation on an HPC cluster or a single PC equipped with a general purpose graphics processing
91 unit (GPGPU).

92 Apart from simulation speed, PDTs have been important in understanding population level behaviour
93 analytically. Important questions, such as 'why are cortical networks stable?' (Amit and Brunel, 1997),
94 'how can a population be oscillatory when its constituent neurons fire sporadically?' (Brunel and Hakim,
95 1999), 'how does spike shape influence the transmission spectrum of a population?' (Fourcaud-Trocmé
96 et al., 2003) have been analysed in the context of population density techniques, providing insights that
97 cannot be obtained from merely running simulations. A particularly important question, which has not been
98 answered in full is: 'how do rate-based equations emerge from populations of spiking neurons and when is
99 their use appropriate?'. There are many situations where such rate-based equations are appropriate, but
100 some where they are not and their correspondence to the underlying spiking neural dynamics is not always
101 clear (Montbrió et al., 2015; de Kamps, 2013). There is a body of work suggesting that some rate-based
102 equations can be seen as the lowest order of perturbations of a stationary state, and much of this work is
103 PDT-based (Wilson and Cowan, 1972; Gerstner, 1998; Mattia and Del Giudice, 2002, 2004; Montbrió
104 et al., 2015). MIIND opens the possibility to incorporate these theoretical insights into large-scale network
105 models. For example, we can demonstrate the prediction from Brunel and Hakim (1999) that inhibitory
106 feedback on a population can cause a bifurcation and produce resonance.
107

108 1.3 Population-level Modeling

109 For the population density approach we take with MIIND, the time evolution of the probability density
110 function is described by a partial integro-differential equation. We give it here to highlight some of its

111 features, but for an in depth introduction to the formalism and a derivation of the central equations we refer
 112 to Omurtag et al. (2000).

$$\frac{\partial \rho}{\partial t} + \frac{\partial}{\partial \vec{v}} \cdot \left(\frac{\vec{F}(\vec{v})\rho(\vec{v}, t)}{\tau} \right) = \int_M d\vec{v}' \left\{ W(\vec{v} \mid \vec{v}')\rho(\vec{v}') - W(\vec{v}' \mid \vec{v})\rho(\vec{v}) \right\}, \quad (1)$$

113 ρ is the probability density function defined over a volume of state space, M , in terms of time, t , and
 114 time-dependent variables, \vec{v} , under the assumption that the neuronal dynamics of a point model neuron is
 115 given by:

$$\tau \frac{d\vec{v}}{dt} = \vec{F}(\vec{v}), \quad (2)$$

116 where τ is the neuron's membrane time constant. Simple models are one-dimensional (1D). For the
 117 leaky-integrate-and-fire (LIF) neuron:

$$F(v) = -v, \quad (3)$$

118 For a quadratic-integrate-and-fire (QIF) neuron:

$$F(v) = v^2 + I, \quad (4)$$

119 where v is the membrane potential, and I can be interpreted as a bifurcation parameter. More complex
 120 models require a higher dimensional state space. Since such a space is hard to visualise and understand,
 121 considerable effort has been invested in the creation of effective models. In particular two-dimensional
 122 (2D) models are considered to be a compromise that allows considerably more biological realism than LIF
 123 or QIF neurons, but which remain amenable to visualisation and analysis, and can often be interpreted
 124 geometrically (Izhikevich, 2007). Examples are the Izhikevich simple neuron (Izhikevich, 2003), the
 125 Fitzhugh-Nagumo neuron (FitzHugh, 1961; Nagumo et al., 1962), and the adaptive-exponential-integrate-
 126 and-fire neuron (Brette and Gerstner, 2005), incorporating phenomena such as bursting, bifurcations,
 127 adaptation, and others that cannot be accounted for in a one dimensional model.

128 $W(v \mid v')$ in Eq. 1 represents a transition probability rate function. The right hand side of Eq. 1 makes it
 129 a Master equation. Any Markovian process can be represented by a suitable choice of W . For example, for
 130 shot noise, we have

$$W(v' \mid v) = \nu(\delta(v' - v - h) - \delta(v - v')), \quad (5)$$

131 where ν is the rate of the Poisson process generating spike events. The delta functions reflect that an
 132 incoming spike causes a rapid change in state space, modeled as an instantaneous jump, h . It depends on the
 133 particular neural model in what variable the jumps take place. Often models use a so-called delta synapse,
 134 such that the jump is in membrane potential. In conductance based models, the incoming spike causes a
 135 jump in the conductance variable (Fig. 1A), and the influence of the incoming spike on the potential is then
 136 indirect, given by the dynamical system's response to the sudden change in the conductance state.

137 MIIND produces a numerical solution to Eq. 1 for arbitrary 1D or 2D versions of $\vec{F}(\vec{v})$ (support for 3D
 138 versions is in development), under a broad variety of noise processes. Indeed, the right hand side of Eq. 1
 139 can be generalised to non-Markov processes which cannot simply be formulated in terms of a transition
 140 probability rate function W . It is possible to introduce a right hand side that entails an integration over a
 141 past history of the density using a kernel whose shape is determined by a non-Markov process (Lai and

142 de Kamps, 2017).

143

144 1.4 Quick Start Guide

145 Before describing the implementation details of MIIND, this section demonstrates how to quickly
 146 set up a simulation for a simple E-I network of populations of conductance based neurons using the
 147 MIIND Python library. A rudimentary level of Python experience is needed to run the simulation. In
 148 most cases, MIIND can be installed via Python pip. Detailed installation instructions can be found in
 149 the *README.md* file of the MIIND repository (De Kamps et al., 2020). For this example, we will use a
 150 pre-written script, *generateCondFiles.py*, to generate the required simulation files which can be found in
 151 the *examples/quick_start* directory of the MIIND repository or can be loaded into a working directory using
 152 the following python command.

153 \$ python -m miind.loadExamples

154 In the *examples/quick_start* directory, the *generateCondFiles.py* script generates the simulation files,
 155 *cond.model* and *cond.tmat*.

156 \$ python generateCondFiles.py

157 The contents of *generateCondFiles.py* is given in Listing 1. The two important parts of the script
 158 are the neuron model function, in this case named *cond()*, and the call to the MIIND function
 159 *grid_generate.generate()* which takes a number of parameters which are discussed in detail later.

Listing 1. *generateCondFiles.py*

```
160 import miind.grid_generate as grid_generate
161
162 def cond(y,t):
163     E_r = -65e-3
164     tau_m = 20e-3
165     tau_s = 5e-3
166
167     v = y[0];
168     h = y[1];
169
170     v_prime = ( -(v - E_r) - (h * v) ) / tau_m
171     h_prime = -h / tau_s
172
173     return [v_prime, h_prime]
174
175 grid_generate.generate(
176     func = cond,
177     timestep = 1e-04,
178     timescale = 1,
179     tolerance = 1e-6,
180     basename = 'cond',
181     threshold_v = -55.0e-3,
182     reset_v = -65e-3,
183     reset_shift_h = 0.0,
184     grid_v_min = -72.0e-3,
185     grid_v_max = -54.0e-3,
186     grid_h_min = -1.0,
187     grid_h_max = 2.0,
```

```

188     grid_v_res = 200,
189     grid_h_res = 200,
190     efficacy_orientation = 'h')

```

191 The *cond()* function should be familiar to those who have used Python numerical integration frameworks
 192 such as *scipy.integrate*. It takes the two time dependent variables defined by $y[0]$ and $y[1]$ and a placeholder
 193 parameter, t , for performing a numerical integration. In the function, the user may define how the derivatives
 194 of each variable are to be calculated. The *generate()* function requires a suitable time step, values for a
 195 threshold and reset if needed, and a description of the extent of the state space to be simulated. With this
 196 structure, the user may define any two dimensional neuron model. The generated files are then referenced
 197 in a second file which describes a network of populations to be simulated. Listing 2 shows the contents of
 198 *cond.xml* describing an E-I network which uses the generated files from *generateCondFiles.py*.

Listing 2. *cond.xml*

```

199 <Simulation>
200   <WeightType>CustomConnectionParameters</WeightType>
201   <Algorithms>
202     <Algorithm type="GridAlgorithm" name="COND" modelfile="cond.model" tau_refractive="0.0"
203       ↪ transformfile="cond_0_0_0_0_.tmat" start_v="-0.065" start_w="0.0" >
204       <TimeStep>1e-04</TimeStep>
205     </Algorithm>
206     <Algorithm type="RateFunctor" name="ExcitatoryInput">
207       <expression>800.</expression>
208     </Algorithm>
209   </Algorithms>
210   <Nodes>
211     <Node algorithm="ExcitatoryInput" name="INPUT_E" type="EXCITATORY_DIRECT" />
212     <Node algorithm="ExcitatoryInput" name="INPUT_I" type="EXCITATORY_DIRECT" />
213     <Node algorithm="COND" name="E" type="EXCITATORY_DIRECT" />
214     <Node algorithm="COND" name="I" type="INHIBITORY_DIRECT" />
215   </Nodes>
216   <Connections>
217     <Connection In="INPUT_E" Out="E" num_connections="1" efficacy="0.1" delay="0.0"/>
218     <Connection In="INPUT_I" Out="I" num_connections="1" efficacy="0.1" delay="0.0"/>
219     <Connection In="E" Out="I" num_connections="1" efficacy="0.1" delay="0.001"/>
220     <Connection In="E" Out="E" num_connections="1" efficacy="0.1" delay="0.001"/>
221     <Connection In="I" Out="E" num_connections="1" efficacy="-0.1" delay="0.001"/>
222     <Connection In="I" Out="I" num_connections="1" efficacy="-0.1" delay="0.001"/>
223   </Connections>
224   <Reporting>
225     <Display node="E" />
226     <Display node="I" />
227     <Rate node="E" t_interval="0.001" />
228     <Rate node="I" t_interval="0.001" />
229   </Reporting>
230   <SimulationRunParameter>
231     <SimulationName>EINetwork</SimulationName>
232     <t_end>0.2</t_end>
233     <t_step>1e-04</t_step>
234     <name_log>einetwork.log</name_log>
235   </SimulationRunParameter>
236 </Simulation>

```

237 The full syntax documentation for MIIND XML files is given in section 4. Though more compact or
238 flexible formats are available, XML was chosen as a formatting style due to its ubiquity ensuring the
239 majority of users will already be familiar with the syntax. The *Algorithms* section is used to declare specific
240 simulation methods for one or more populations in the network. In this case, a GridAlgorithm named
241 *COND* is set up which references the *cond.model* and *cond.tmat* files. A RateFunctor algorithm produces a
242 constant firing rate. In the *Nodes* section, two instances of *COND* are created: one for the excitatory and
243 inhibitory populations respectively. Two *ExcitatoryInput* nodes are also defined. The *Connections* section
244 allows us to connect the input nodes to the two conductance populations. The populations are connected to
245 each other and to themselves with a 1ms transmission delay. The remaining sections are used to define how
246 the output of the simulation is to be recorded, and to provide important simulation parameters such as the
247 simulation time. By running the following python command, the simulation can be run.

Listing 3. Run the cond.xml simulation.

248 \$ python -m miind.run cond.xml

249 The probability density plots for both populations will be displayed in separate windows as the simulation
250 progresses. The firing rate of the excitatory population can be plotted using the following commands. Fig.
251 2 shows the probability density plots for both populations and average firing rate of population E.

Listing 4. Load the cond.xml simulation and plot the average firing rate of population E.

252 \$ python -m miind.miindio sim cond.xml
253 \$ python -m miind.miindio rate E

254 Finally, the density function of each population can be plotted as a heat map for a given time in the
255 simulation.

Listing 5. Plot the probability density of population I at time 0.12s.

256 \$ python -m miind.miindio plot-density I 0.12

257 Later sections will show how the MIIND simulation can be imported into a user defined Python script
258 so that input can be dynamically set during simulation and population activity can be captured for further
259 processing.

2 THE MIIND GRID ALGORITHM

260 MIIND allows the user to simulate populations of any 1D or 2D neuron model. Although much of MIIND's
261 architecture is agnostic to the integration technique used to simulate each population, the system is primarily
262 designed to make use of its novel population density techniques, grid algorithm and mesh algorithm. Both
263 algorithms use a discretisation of the underlying neuron model's state space such that each discrete "cell",
264 which covers a small area of state space, is considered to hold a uniform distribution of probability mass.
265 In both algorithms, MIIND performs three important steps for each iteration. First, probability mass is
266 transferred from each cell to one or more other cells according to the dynamics of the underlying neuron
267 model in the absence of any input. The probability mass is then spread across multiple other cells due to
268 incoming random spikes. Finally, if the underlying neuron model has a threshold-reset mechanic, such as
269 an integrate and fire model, probability mass which has passed the threshold is transferred to cells along
270 the reset potential. As it is the most practically convenient method for the user, we will first introduce the
271 grid algorithm. We will discuss its benefits and weaknesses, indicating where it may be appropriate to use
272 the mesh algorithm instead.

273

274 2.1 Generating the Grid and Transition Matrix

275 To discretise the state space in the grid method, the user can specify the size and $M \times N$ resolution of
 276 a rectangular grid which results in MN identical rectangular cells, each of which will hold probability
 277 mass. In the grid algorithm, a transition matrix lists the proportion of mass which moves from each cell to
 278 (usually) adjacent cells in one time step due to the deterministic dynamics of the underlying neural model.
 279 To pre-calculate the transitions for each cell, MIIND first translates the vertices of every cell by integrating
 280 each point forward by one time step according to the dynamics of the underlying neuron model as shown
 281 in Fig. 3A. As the time step is small, a single Euler step is usually all that is required to avoid large errors
 282 (although other integration schemes can be used if required). Each transformed cell is no longer guaranteed
 283 to be a rectangle and is compared to the original non-transformed grid to ascertain which cells overlap with
 284 the newly generated quadrilateral. An overlap indicates that some proportion of neurons in the original
 285 cell will move to the overlapping cell after one time step. In order to calculate the overlap, the algorithm
 286 in Listing 6 is employed. This algorithm is also used in the geometric method of generating transition
 287 matrices for the mesh algorithm shown later.

Listing 6. A pseudo-code representation of the algorithm used to calculate the overlapping areas between transformed grid cells and the original grid (or for translated cells of a mesh). The proportion of the area of the original cell gives the proportion of probability mass to be moved in each transition.

```
288 For each transformed cell, A, in the grid:
289   Translate all four vertices according to a single Euler step.
290   Split A into two triangles and add them to a triangle list.
291 For each non-transformed cell, B:
292   Set the overlapping area sum to 0.
293   While the triangle list has changed:
294     For each triangle in the list:
295       If the triangle is entirely outside B: add 0 to the sum.
296       If the triangle is entirely within B: add the triangle's area to the sum.
297       If B is entirely within the triangle: add B's area to the sum.
298       Else: For each edge in B:
299         Calculate any intersection points with the edges of the triangle.
300         Triangulate the polygon produced by the original triangle points plus the new intersection
301           ↪ points.
302         Remove the original triangle from the list.
303         Add the newly generated triangles to the list.
304       Calculate the proportion of A taken by the sum.
305       Add the transition from A to B with the proportion to the transition matrix.
```

306 Though the pseudo-code algorithm is order N^2 , there are many ways that the efficiency of the algorithm
 307 is improved in the implementation. The number of non-transformed cells checked for overlap can be limited
 308 to only those which lie underneath each given triangle. Furthermore, the outer loop is parallelisable. Finally,
 309 as the non-transformed cells are axis-aligned rectangles, the calculation to find edge intersections is trivial.
 310 Fig. 3A shows a fully translated and triangulated cell at the end of the algorithm. Once the transition matrix
 311 has been generated, it is stored in a file with the extension *.tmat*. Although the regular grid can be described
 312 with only four parameters (the width, height, X, and Y resolutions), to more closely match the behaviour of
 313 mesh algorithm, the vertices of the grid are stored in a *.model* file. To simulate a population using the grid
 314 algorithm, the *.tmat* and *.model* files must be generated and referenced in the XML simulation file.
 315

316 As demonstrated in the quick start guide (section 1.4), to generate a *.model* and *.tmat* file, the user must
317 write a short Python script which defines the underlying neuron model and makes a call to the MIIND API
318 to run the algorithm in listing 6. In the *python* directory of the MIIND source repository (see section 1
319 in the supplementary material), there are a number of examples of these short scripts. The script used to
320 generate a grid for the Izhikevich simple model is listed in the supplementary material section 9.1. The
321 required definition of the neuron model function is similar to those used by many numerical integration
322 libraries. The function takes a parameter, *y*, which represents a list which holds the two time dependent
323 variables and a parameter, *t*, which is a placeholder for use in integration. The function must return the first
324 time derivatives of each variable as a list in the same order as in *y*. Once the function has been written, a
325 call to *grid_generate.generate* is made which takes the parameters listed in Table 1.

326 When the user runs the script, the required *.model* and *.tmat* files will be generated for use in a simulation.
327 In the quick start guide, the conductance based neuron model requires that *efficacy_orientation* is set to
328 ‘h’ because incoming spikes cause an instantaneous change in the conductance variable instead of the
329 membrane potential. By default, however, this parameter is set to ‘v’. When choosing values for the grid
330 bounds (*grid_v_min*, *grid_v_max*, *grid_h_min*, and *grid_h_max*), the aim is to estimate where in state space
331 the population density function might be non-zero during a simulation. In the conductance based neuron
332 model, because of the threshold-reset mechanic, the *grid_v_max* parameter need only be slightly above
333 the threshold to ensure that there is at least one column of cells on or above threshold to allow probability
334 mass to be reset. The *grid_v_min* value should be below the resting potential and reset potential. However,
335 we must also consider that the neurons could receive inhibitory spikes which would cause the neurons to
336 hyperpolarise. *grid_v_min* should therefore be set to a value beyond the lowest membrane potential expected
337 during the simulation. Similarly for the conductance variable, space should be provided for reasonable
338 positive and negative values. If it is known beforehand that no inhibition will occur, however, then the state
339 space bounds can be set tighter in order to improve the accuracy of the simulation using the same grid
340 resolution (*grid_v_res* and *grid_h_res*). If, during the simulation, probability mass is pushed beyond the
341 lower bounds of the grid, it will be pinned at those lower bounds which will produce incorrect behaviour
342 and results. If the probability mass is pushed beyond the upper bounds, it will be wrapped around to the
343 lower bounds which will also produce incorrect results. The choice of grid resolution is a balance between
344 speed of simulation and accuracy. However, even very coarse grids can produce representative firing rates
345 and behaviours. Typical grid resolutions range between 100x100 and 500x500. It can also be beneficial
346 to experiment with different *M* and *N* values as the accuracy of each dimension can have unbalanced
347 **The Effect of Random Incoming Spikes**

348 The transition matrix in the *.tmat* file describes how probability mass moves to other cells due to the
349 deterministic dynamics of the underlying neuron model. The transition matrix is sparse as probability mass
350 is often only transferred to nearby cells. Solving the deterministic dynamics is therefore very efficient. The
351 mesh algorithm is even faster and, as demonstrated later, is significantly quicker than direct simulation
352 for this part of the algorithm. Another benefit to the modeler is that by rendering the grid with each cell
353 coloured according to its mass, the resultant heat map gives an excellent visualisation of the state of the
354 population as a whole at each time step of the simulation as shown in Fig. 2. This provides particularly
355 useful insight into the sub-threshold behaviour of neurons in the population.
356

359 The second step of the grid algorithm, which must be performed every iteration, is to solve the change
 360 in the probability density function due to random incoming spikes. It is assumed that a spike causes an
 361 instantaneous change in the state of a neuron, usually a step wise jump in membrane potential corresponding
 362 to a constant synaptic efficacy. In the conductance based neuron example, this jump is in the conductance.
 363 When considering each cell in the grid, a single incoming spike will cause some proportion of the
 364 probability mass to shift to at most, two other cells as shown in Fig. 3. Because all cells in the grid are
 365 equally distributed and the same size, the relative transition of probability mass caused by a single spike is
 366 the same for them all. A sparse transition matrix, M , can be generated from this single transition so that
 367 applying M to the probability density grid applies the transition to all cells. MIIND calculates a different
 368 M for each incoming connection to the population based on the user defined instantaneous jump, which
 369 we refer to as the efficacy. In the mesh algorithm, the relative transitions are different for each cell and so a
 370 transition matrix (similar to that of the *.tmat* file) is required to describe the effect of a single spike. As with
 371 many other population density techniques, MIIND assumes that incoming spikes are Poisson distributed,
 372 although it is possible to approximate other distributions. MIIND uses M to calculate the change to the
 373 probability density function, ρ , due solely to the non-deterministic dynamics as described by equation 6.

$$d\rho/dt = \lambda M \rho \quad (6)$$

374 λ is the incoming Poisson firing rate. The boost numeric library is used to integrate $d\rho/dt$. The solution
 375 to this equation describes the spread of the probability density due to Poisson spikes. This ‘master process’
 376 step amounts to multiple applications of the transition matrix M and is where the majority of time is taken
 377 computationally. However, OpenMP is available in MIIND to parallelise the matrix multiplication. If
 378 multiple cores are available, the OpenMP implementation significantly improves performance of the master
 379 process step. More information covering this technique can be found in De Kamps et al. (2019); de Kamps
 380 (2013).

382 2.3 Threshold-Reset Dynamics

383 Many neuron models include a “threshold-reset” process such that neurons which pass a certain mem-
 384 brane potential value are shifted back to a defined reset potential to approximate repolarisation during an
 385 action potential. To facilitate this in MIIND, after each iteration, probability mass in cells which lie across
 386 the threshold potential is relocated to cells which lie across the reset potential according to a pre-calculated
 387 mapping. Often, a refractory period is used to hold neurons at the reset potential before allowing them to
 388 again receive incoming spikes. In MIIND this is implemented using a queue for each threshold cell as
 389 shown in Fig. 4. The queues are set to the length of the refractory period divided by the time step, rounded
 390 up to the nearest integer value. During each iteration, probability mass is shifted one position along the
 391 queue. A linear interpolation of the final two places in the queue is made and this value is passed to the
 392 mapped reset cell. The interpolation is required in case the refractory period is not an integer multiple of
 393 the time step. The total probability mass in the threshold cells each iteration is used to calculate the average
 394 population firing rate. For models which do not require threshold-reset dynamics, setting the threshold
 395 value to the maximal membrane potential of the grid, and the reset to the minimal membrane potential
 396 ensures that no resetting of probability mass will occur.

397

398 2.4 How MIIND Facilitates Interacting Populations

399 The grid algorithm describes how the behaviour of a single population is simulated. The MIIND software
400 platform as a whole provides a way for many populations with possibly many different integration algo-
401 rithms to interact in a network. The basic process of simulating a network is as follows. The user must
402 write an XML file which describes the whole simulation. This includes defining the population nodes of
403 the network and how they are connected; which integration technique each population uses (grid algorithm,
404 mesh algorithm etc.); external inputs to the network; how the activity of each population will be recorded
405 and displayed; the length and time step of the simulation. As shown in the quick start guide, the XML file
406 can be passed as a parameter to the *miind.run* module in Python. When the simulation is run, a population
407 network is instantiated and the simulation loop is started. For each iteration, the output activity of each
408 population node is recorded. By default, the activity is assumed to be an average firing rate but other options
409 are available such as average membrane potential. The outputs are passed as inputs to each population node
410 according to the connectivity defined in the XML file. Each population is evolved forward by one time
411 step and the simulation loop repeats until the simulation time is up. The Python front end, *miind.miindio*,
412 provides the user with tools to analyse the output from the simulation. A custom *run* script can also be
413 written by the user to perform further analysis and processing.
414

415 The simplicity of the XML file means that a user can set up a large network of populations with very
416 little effort. The model archive in the code repository holds a set of example simulations demonstrating the
417 range of MIIND’s functionality and includes an example which simulates the Potjans-Diesmann model
418 of a cortical microcircuit (Potjans and Diesmann, 2014), which is made up of eight populations of leaky
419 integrate and fire neurons. Fig. 5 shows a representation of the model with embedded density plots for each
420 population.
421

422 2.5 Running MIIND Simulations

423 The quick start guide demonstrated the simplest way to run a simulation given that the required *.model*,
424 *.tmat*, and *.XML* files have been generated. The *miind.run* script imports the *miind.miindsim* Python
425 extension module which can also be imported into any user written Python script. Section 6 details the
426 functions which are exposed by *miind.miindsim* for use in a python script. The benefit of this method is
427 that the outputs from populations can be recorded after each iteration and inputs can be dynamic allowing
428 the python script to perform its own logic on the simulation based on the current state.
429 There is also a command line interface (CLI) program provided by the Python module, *miind.miindio*. The
430 CLI can be used for many simple work flow tasks such as generating models and displaying results. Each
431 command which is available in the CLI, can also be called from the MIIND Python API, upon which the
432 CLI is built. A full list of the available commands in the CLI is given in section 9.3 of the supplementary
433 material and a worked example using common CLI commands is provided in section 7.
434

435 2.6 When not to use the Grid Algorithm

436 For many underlying neuron models, the grid algorithm will produce results showing good agreement
437 with direct simulation to a greater or lesser extent depending on the resolution of the grid (see Fig. 6).
438 However, for models such as exponential integrate and fire, a significantly higher grid resolution is required
439 than might be expected because of the speed of the dynamics across the threshold (beyond which, neurons
440 perform the action potential). When the input rate is high enough to generate tonic spiking in an exponential
441 integrate and fire model, the rate of depolarisation of each neuron reduces as it approaches the threshold

442 potential then once it is beyond the threshold, quickly increases producing a spike. Because the grid
443 discretises the state space into regular cells, if cells are large due to a low resolution, only a small number
444 of cells will span the threshold, as shown in Fig. 7A. When the transition matrix is applied each time
445 step, probability mass is distributed uniformly across each cell. Probability mass can therefore artificially
446 cross the threshold much faster than it should leading to a higher than expected average firing rate for the
447 population. Using the grid algorithm for such models where the firing rate itself is dependent on sharp
448 changes in the speed of the dynamics should be avoided if high accuracy is required. Other neuron models,
449 like the bursting Izhikevich simple model, also have sharp changes in speed when neurons transition from
450 bursting to quiescent periods. However, the bursting firing rate is unaffected by these dynamics and the
451 oscillation frequency is affected only negligibly due to the difference in timescales. The grid algorithm
452 is therefore still appropriate in cases such as this. For exponential integrate and fire models, however,
453 MIIND provides a second algorithm which can more accurately capture the deterministic dynamics: mesh
454 algorithm.

3 THE MIIND MESH ALGORITHM

455 Instead of a regular grid to discretise the state space of the underlying neuron model, the mesh algorithm
456 requires a two dimensional mesh which describes the dynamics of the neuron model itself in the absence
457 of incoming spikes. A mesh is constructed from strips which follow the trajectories of neurons in state
458 space (Fig. 8). The trajectories form so-called characteristic curves of the neuron model from which this
459 method is inspired (De Kamps et al., 2019; de Kamps, 2013).

460 These trajectories are computed as part of a one-time preprocessing step using an appropriate integration
461 technique and time step. Strips will often approach or recede from nullclines and stationary points and
462 their width may shrink or expand according to their proximity to such elements. Each strip is split into
463 cells. Each cell represents how far along the strip neurons will move in a single time step. As with the
464 width of the strips, cells will become more dense or more sparse as the dynamics slow down and speed up
465 respectively. The result of covering the state space with strips is a precomputed description of the model
466 dynamics such that the state of a neuron in one cell of the mesh is guaranteed to be in the next cell along
467 the strip after a single time step. Depending on the underlying neuron model, it can be difficult to get full
468 coverage without cells becoming too small or shear. However, once built, the deterministic dynamics have
469 effectively been “pre-solved” and baked into the mesh.
470

471 As with the grid algorithm, when the simulation is running, each cell is associated with a probability
472 mass value which represents the probability of finding a neuron from the population with a state in that
473 cell. When a probability density function (PDF) is defined across the mesh, computing the change to the
474 PDF due to the deterministic dynamics of the neurons is simply a matter of shifting each cell’s probability
475 mass value along its strip. In the C++ implementation, this requires no more than a pointer update and is
476 therefore quicker than the grid algorithm for solving the deterministic dynamics as no transition matrix is
477 applied to the cells.
478

479 Mesh algorithm does, however, still require a transition matrix to implement the effect of incoming spikes
480 on the PDF. This transition matrix describes how the state of neurons in each cell are translated in the event
481 of a single incoming spike. Unlike the grid algorithm, cells are unevenly distributed across the mesh and
482 are different sizes and shapes. What proportion of probability mass is transferred to which cells with a
483 single incoming spike is, therefore, different for all cells. During simulation, the total change in the PDF is

484 calculated by shifting probability mass one cell down each strip and using the transition matrix to solve the
485 master equation every time step. The combined effect can be seen in Fig. 9. The method of solving the
486 master equation is explained in detail in de Kamps (2013).

487

488 3.1 When not to use the Mesh Algorithm

489 Just as with the grid algorithm, certain neuron models are better suited to an alternative algorithm. In
490 the mesh algorithm, very little error is introduced for the deterministic dynamics. Probability mass flows
491 down each strip as it would without the discretisation and error is limited only to the size of the cells.
492 When the master equation is solved, however, probability mass can spread to parts of state space which
493 would see less or no mass. Fig. 7B demonstrates how in the mesh algorithm, as probability mass is pushed
494 horizontally, very shear cells can allow mass to be incorrectly transferred vertically as well. In the the
495 grid algorithm, error is introduced in the opposite way. Solving the master equation pushes probability
496 mass along horizontal rows of the grid and error is limited to the width of the row. The grid algorithm is
497 preferable over the mesh algorithm for populations of neurons with one fast variable and one slow variable
498 which can produce very shear cells in a mesh, e.g. in the Fitzhugh-Nagumo model (De Kamps et al., 2019).
499 In both algorithms, the error can be reduced by increasing the density of cells (by increasing the resolution
500 of the grid, or by reducing the timestep and strip width of the mesh). However, better efficiency is achieved
501 by using the appropriate algorithm.

502

503 3.2 Building a Mesh for the Mesh Algorithm

504 Before a simulation can be run for a population which uses the mesh algorithm, the pre-calculation steps
505 of generating a mesh and transition matrices must be performed. Fig. 10 shows the full pre-processing
506 pipeline for mesh algorithm. The mesh is a collection of strips made up of quadrilateral cells. As mentioned
507 earlier, probability mass moves along a strip from one cell to the next each time step which describes
508 the deterministic dynamics of the model. Defining the cells and strips of a 2D mesh is not generally a
509 fully automated process and the points of each quadrilateral must be defined by the mesh developer and
510 stored in a *.mesh* file. When creating the mesh, the aim is to cover as much of the state space as possible
511 without allowing cells to get too small or misshapen. An example of a full mesh generation script for
512 the Izhikevich simple neuron model (Izhikevich, 2003) is available in section 9.1 of the supplementary
513 material. MIIND provides *miind.miind_api.LifMeshGenerator*, *miind.miind_api.QifMeshGenerator*, and
514 *miind.miind_api.EifMeshGenerator* scripts to automatically build the 1D leaky integrate and fire, quadratic
515 integrate and fire, and exponential integrate and fire neuron meshes respectively. They can be called from
516 the CLI. The scripts generate the three output files which any mesh generator script must produce: a *.mesh*
517 file, a *.stat* file which defines extra cells in the mesh to hold probability mass that has settled at a stationary
518 point, and a *.rev* file which defines a “reversal mapping” indicating how probability mass is transferred
519 from strips in the mesh to the stationary cells. More information on *.mesh*, *.stat*, and *.rev* files is provided
520 in the supplementary material section 6.

521

522 Once the *.mesh*, *.stat*, and *.rev* files have been generated by the user or by one of the automated 1D
523 scripts, the Python command line interface, *miind.miindio*, provides commands to convert the three files
524 into a single *.model* file and generate transition matrices stored in *.mat* files. The model file is what will be
525 referenced and read by MIIND to load a mesh for a simulation. To generate this file, use the CLI command,
526 **generate-model**. The command parameters are shown in Table 2. All input files must have the same base
527 name, for example: *lif.mesh*, *lif.stat*, and *lif.rev*. If the command runs successfully, a new file will be created:

528 *basename.model*. A number of pre-generated models are available in the *examples* directory of the MIIND
529 repository to be used “out of the box” including the adaptive exponential integrate and fire and conductance
530 based neuron models.

Listing 7. Generate a Model in the CLI

531 > generate-model lif -60.0 -30.0

532 The generated *.model* file contains the mesh vertices, some summary information such as the time step
533 used to generate the mesh and the threshold and reset values, and a mapping of threshold cells to reset cells.
534

535 In the the mesh algorithm, transition matrices are used to solve the Poisson master equation which
536 describes the movement of probability mass due to incoming random spikes. In the mesh algorithm, one
537 transition matrix is required for each post synaptic efficacy that will be needed in the simulation. So if a
538 population is going to receive spikes which cause jumps of 0.1mV and 0.5mV, two transition matrices are
539 required. It is demonstrated later how the efficacy can be made dependent on the membrane potential or
540 other variables. Each transition matrix is stored in a *.mat* file and contains a list of source cells, target cells,
541 and proportions of probability mass to be transferred to each. For a given cell in the mesh, neurons with a
542 state inside that cell which receive a single external spike will shift their location in state space by the value
543 of the efficacy. Neurons from the same cell could therefore end up in many other different cells, though
544 often ones which are nearby. It is assumed that neurons are distributed uniformly across the source cell.
545 Therefore, the proportion of neurons which end up in each of the other cells can be calculated. MIIND
546 performs this calculation in two ways, the choice for which is given to the user.
547

548 The first method is to use a Monte Carlo approach such that a number of points are randomly placed in
549 the source cell then translated according to the efficacy. A search takes place to find which cells the points
550 were translated to and the proportions are calculated from the number of points in each. For many meshes,
551 a surprisingly small number of points, around 10, is required in each cell to get a good approximation
552 for the transition matrix and the process is therefore quite efficient. As shown in Fig. 10, an additional
553 process is required when generating transition matrices using Monte Carlo which includes two further
554 intermediate files, *.fid* and *.lost*. All points must be accounted for when performing the search and in cases
555 where points are translated outside of the mesh, an exhaustive search must be made to find the closest cell.
556 The **lost** command allows the user to speed up this process which is covered in detail in section 6.1 of the
557 supplementary material.
558

559 The second method translates the actual vertices of each cell according to the efficacy and calculates the
560 exact overlapping area with other cells. The method by which this is achieved is the same as that used to
561 generate the transition matrix of the grid algorithm, described in section 2.1. This method provides much
562 higher accuracy than Monte Carlo but is one order of magnitude slower (it takes a similar amount of time
563 to perform Monte Carlo with 100 points per cell). For some meshes, it is crucial to include very small
564 transitions between cells to properly capture the dynamics which justifies the need for the slower method.
565 It also benefits from requiring no additional user input in contrast to the Monte Carlo method.
566

567 In *miind.miindio*, the command **generate-matrix** can be used to automatically generate each *.mat*
 568 file. In order to work, there must be a *basename.model* file in the working directory. The **generate-**
 569 **matrix** command takes six parameters which are described in Table 3. Listing 8 shows an example of the
 570 **generate-matrix** command. If successful, two files are generated: *basename.mat* and *basename.lost*.

Listing 8. The *miind.miindio* command to generate a matrix using the *adex.model* file with an efficacy of 0.1 in *v* and a jump of 5.0 in *w* when a neuron spikes. The Monte Carlo method has been chosen with 10 points per cell.

571 > generate-matrix adex 0.1 10 0.0 5.0 false

572 Once **generate-matrix** has completed, a *.mat* file will have been generated and the *.model* file will have
 573 been amended to include a *<Reset Mapping>* section. Similar to the reversal mapping in the *.rev* file,
 574 the reset mapping describes movement of probability mass from the cells which lie across the threshold
 575 potential to cells which lie across the reset potential. If the threshold or reset values are changed but no
 576 other change is made to the mesh, it can be helpful to re-run the mapping calculation without having
 577 to completely re-calculate the transition matrix. *miind.miindio* provides the command **regenerate-reset**
 578 which takes the base name and any new reset shift value (0 if not required) as parameters. This will quickly
 579 replace the reset mapping in the *.model* file.

Listing 9. The user may change the *<Threshold>* and *<Reset>* values in the *.model* file (or re-call **generate-model** with different threshold and reset values) then update the existing Reset Mapping. In this case, the *adex.model* was updated with a reset *w* shift value of 7.0.

580 > regenerate-reset adex 7.0

581 With all required files generated, a simulation using the mesh algorithm can now be run in MIIND.

582

583 3.3 Jump Files

584 In some models, it is helpful to be able to set the efficacy as a function of the state. For example,
 585 to approximate adaptive behaviour where the post synaptic efficacy lowers as the membrane potential
 586 increases. Jump files have been used in MIIND to simulate the Tsodyks-Markram (Tsodyks and Markram,
 587 1997) synapse model as described in De Kamps et al. (2019). In the model, one variable/dimension is
 588 required to represent the membrane potential, *V*, of the post-synaptic neuron and the second to represent
 589 the synaptic contribution, *G*. *G* and *V* are then used to derive the post-synaptic potential caused by an
 590 incoming spike. Before generating the transition matrix, each cell can be assigned its own efficacy for
 591 which the transitions will be calculated. During generation, Monte Carlo points will be translated according
 592 to that value instead of a constant across the entire mesh. When calling the **generate-matrix** command, a
 593 separate set of three parameters is required to use this feature. The base name of the model file, the number
 594 of Monte Carlo points per cell, and a reference to a *.jump* file which stores the efficacy values for each cell
 595 in the mesh.

Listing 10. Generate a transition matrix with a jump file in the CLI

596 > generate-matrix adex 10 adex.jump

597 As with the files required to build the mesh, the jump file must be user generated as the efficacy values may
 598 be non-linear and involve one or both of the dimensions of the model. The format of a jump file is shown
 599 in listing 11. The *<Efficacy>* element of the XML file gives an efficacy value for both dimensions of the

600 model and is how the resulting transition matrix will be referenced in the simulation. The *<Translations>*
 601 element lists the efficacy in both dimensions for each cell in the mesh.

Listing 11. The format of the jump file. Each line in the *<Translations>* block gives the strip,cell coordinates of the cell followed by the *h* efficacy then the *v* efficacy. The *<Efficacy>* element gives a reference efficacy which will be used to reference the transition matrix built with this jump file. It must therefore be unique among jump files used for the same model.

```
602 <Jump>
603 <Efficacy>0.0 0.1</Efficacy>
604 <Translations>
605 0,0 0.0 0.1
606 1,0 0.0 0.1
607 1,1 0.0 0.10012
608 1,2 0.0 0.10045
609 ...
610 </Translations>
611 </Jump>
```

612 After calling **generate-matrix**, as before, the *.mat* file will be created with the quoted values in the
 613 *<Efficacy>* element of the jump file. As with the vanilla Monte Carlo generation, the additional process of
 614 tracking lost points must be performed.

615

4 WRITING THE XML FILE

616 MIIND provides an intuitive XML style language to describe a simulation and its parameters. This includes
 617 descriptions of populations, neuron models, integration techniques, and connectivity as well as general
 618 parameters such as time step and duration. The XML file is split into sections which are sub elements of
 619 the XML root node, *<Simulation>*. They are Algorithms, Nodes, Connections, Reporting, and Simulation-
 620 RunParameter. These elements make up the major components of a MIIND simulation.

621

4.1 Algorithms

622 An *<Algorithm>* in the XML code describes the simulation method for a population in the network. The
 623 nodes of the network represent separate instances of these algorithm elements. Therefore, many nodes can
 624 use the same algorithm. Each algorithm has different parameters or supporting files but as a minimum, all
 625 algorithms must declare a type and a name. Each algorithm is also implicitly associated with a “weight
 626 type”. All algorithms used in a single simulation must be compatible with the weight type as it describes the
 627 way that populations interact. The *<WeightType>* element of the XML file can take the values, “double”,
 628 “DelayedConnection”, or “CustomConnectionParameters”. Which value the weight type element takes
 629 influences which algorithms are available in the simulation and how the connections between populations
 630 will be defined. The following sections cover all Algorithm types currently supported in MIIND. Table 4
 631 lists these algorithms and their compatible weight types.

632

4.1.1 RateAlgorithm

633 RateAlgorithm is used to supply a Poisson distributed input (with a given average firing rate) to other
 634 nodes in the simulation. It is typically used for simulating external input. The *<rate>* sub-element is used
 635 to define the activity value which is usually a firing rate.

Listing 12. A RateAlgorithm definition with a constant rate of 100Hz.

```

638 <Algorithm name="Cortical Background Algorithm" type="RateAlgorithm">
639   <rate>100.0</rate>
640 </Algorithm>
```

4.1.2 MeshAlgorithm and MeshAlgorithmCustom

641 In section 3.2, we saw how to generate *.model* and *.mat* files. These are required to simulate a population
 642 using the mesh algorithm. Algorithm type=MeshAlgorithm tells MIIND to use this technique. The model
 643 file is referenced as an attribute to the Algorithm definition. The *TimeStep* child element must match that
 644 which was used to generate the mesh. This value is quoted in the model file. As many *MatrixFile* elements
 645 can be declared as are required for the simulation, each with an associated .mat file reference.

Listing 13. A MeshAlgorithm definition with two matrix files.

```

647 <Algorithm type="MeshAlgorithm" name="ALG_ADEX" modelfile="adex.model" >
648   <TimeStep>0.001</TimeStep>
649   <MatrixFile>adex_0.05_0_0_0_.mat</MatrixFile>
650   <MatrixFile>adex_-0.05_0_0_0_.mat</MatrixFile>
651 </Algorithm>
```

652 MeshAlgorithm provides two further optional attributes in addition to *modelfile*. The first is *tau_refractive*
 653 which enables a refractory period and the second is *ratemethod* which takes the value “AvgV” if the activity
 654 of the population is to be represented by the average membrane potential. Any other value for *ratemethod*
 655 will set the activity to the default average firing rate. The activity value is what will be passed to other
 656 populations in the network as well as what will be recorded as the activity for any populations using this
 657 algorithm.

658 When the weight type is set to CustomConnectionParameters, the type of this algorithm definition should
 659 be changed to MeshAlgorithmCustom. No other changes to the definition are required.

660

4.1.3 GridAlgorithm and GridJumpAlgorithm

661 For populations which use the grid algorithm, the following listing is required. Similar to the MeshAl-
 662 gorithm, the model file is referenced as an attribute. However, there are no matrix files required as the
 663 transition matrix for solving the Poisson master equation is calculated at run time. The transition matrix
 664 for the deterministic dynamics, stored in the *.tmat* file, is referenced as an attribute as well. Attributes for
 665 *tau_refractive* and *ratemethod* are also available with the same effects as for MeshAlgorithm.

Listing 14. A GridAlgorithm definition using the AvgV (membrane potential) rate method.

```

667 <Algorithm type="GridAlgorithm" name="GRIDALG_FN" modelfile="fn.model" tau_refractive="0.0"
668   ↳ transformfile="fn_0_0_0_0_.tmat" start_v="-1.0" start_w="-0.3" ratemethod="AvgV">
669 <TimeStep>0.00001</TimeStep>
670 </Algorithm>
```

671 GridAlgorithm also provides additional attributes *start_v* and *start_w* which allows the user to set the
 672 starting state of all neurons in the population which creates an initial probability mass of 1.0 in the
 673 corresponding grid cell at the start of the simulation.

674 GridJumpAlgorithm provides a similar functionality as MeshAlgorithm when the transition matrix is
 675 generated using a jump file. That is, the efficacy applied to each cell when calculating transitions differs
 676 from cell to cell. In GridJumpAlgorithm, the efficacy at each cell is multiplied by the distance between
 677 the central *v* value of the cell and a user defined “stationary” value. The initial efficacy and the stationary

678 values are defined by the user in the XML `<Connection>` elements. GridJumpAlgorithm is useful for
 679 approximating populations of neurons with a voltage dependent synapse.

Listing 15. A GridJumpAlgorithm definition and corresponding Connection with a “stationary” attribute. The efficacy at each grid cell will equal the original efficacy value (-0.05) multiplied by the difference between each cell’s central v value and the given stationary value (-65)

```
680 <Algorithm type="GridJumpAlgorithm" name="ALG_ADEX" modelfile="adex.model" tau_refractive="0.0"
681   ↪ transformfile="adex_0_0_0_0_.tmat" start_v="-65.0" start_w="0.0">
682 <TimeStep>0.0001</TimeStep>
683 </Algorithm>
684 ...
685 <Connection In="BG_NOISE" Out="ADEX_NODE" num_connections="1" efficacy="-0.05" delay="0.0" stationary=
686   ↪ -65.0"/>
```

687 4.1.4 Additional Algorithms

688 MIIND also provides OUAlgorithm and WilsonCowanAlgorithm. The OUAlgorithm generates an
 689 Ornstein–Uhlenbeck process (Uhlenbeck and Ornstein, 1930) for simulating a population of LIF neurons.
 690 The WilsonCowanAlgorithm implements the Wilson–Cowan model for simulating population activity
 691 (Wilson and Cowan, 1972). Examples of these algorithms are provided in the examples directory of the
 692 MIIND repository (*examples/twopop* and *examples/model_archive/WilsonCowan*).
 693 One final algorithm, RateFunctor, behaves similarly to RateAlgorithm. However, instead of a rate value, the
 694 child value defines the activity using a C++ expression in terms of variable, *t*, representing the simulation
 695 time.

Listing 16. A RateFunctor algorithm definition in which the firing rate linearly increases to 100Hz over 0.1 seconds and remains at 100Hz thereafter.

```
696 <Algorithm type="RateFunctor" name="ExternalInput">
697   <expression><! [CDATA[ t < 0.1 ? (t/0.1)*100 : 100 ]]></expression>
698 </Algorithm>
```

699 A CDATA expression is not permitted when using MIIND in Python or when calling *miind.run*. However,
 700 RateFunctor can still be used with a constant expression (although this has no benefit beyond what RateAl-
 701 gorithm already provides). CDATA should only be used when MIIND is built from source (not installed
 702 using pip) and the MIIND API is used to generate C++ code from an XML file.
 703

704 4.2 Nodes

705 The `<Node>` block lists instances of the Algorithms defined above. Each node represents a single
 706 population in the network. To create a node, the user must provide the name of one of the algorithms
 707 defined in the algorithm block which will be instantiated. A name must also be given to uniquely identify
 708 this node. The type describes the population as wholly inhibitory, excitatory, or neutral. The type dictates
 709 the sign of the post synaptic efficacy caused by spikes from this population. Setting the type to neutral
 710 allows the population to produce both excitatory and inhibitory (positive and negative) synaptic efficacies.
 711 For most algorithms, the valid types for a node are *EXCITATORY*, *INHIBITORY*, and *NEUTRAL*. *EXCITA-*
TORY_DIRECT and *INHIBITORY_DIRECT* are also available but mean the same as *EXCITATORY* and
 713 *INHIBITORY* respectively.

Listing 17. Three nodes defined in the Nodes section using the types *NEUTRAL*, *INHIBITORY*, and *EXCITATORY* respectively.

```
714 <Nodes>
```

```

715 ...
716 <Node algorithm="GRIDALG_FN" name="POP_1" type="NEUTRAL" />
717 <Node algorithm="ALG_ADEX" name="ADEX_NODE" type="INHIBITORY" />
718 <Node algorithm="RATEFUNC_BACKGROUND" name="BG_NOISE" type="EXCITATORY" />
719 ...
720 </Nodes>
```

721 Many nodes can reference the same algorithm to use the same population model but they will behave
 722 independently based on their individual inputs.

723

724 4.3 Connections

725 The connections between the nodes are defined in the *<Connections>* sub-element. Each connection
 726 can be thought of as a conduit which passes the output activity from the “In” population node to the “Out”
 727 population node. The format used to define the connections is dependent on the choice of *WeightType*.
 728 When the type is *double*, connections require a single value which represents the connection weight. This
 729 will be multiplied by the output activity of the In population and passed to the Out population. The sign of
 730 the weight must match the In node’s type definition (*EXCITATORY*, *INHIBITORY*, *NEUTRAL*).

Listing 18. A simple double WeightType Connection with a single rate multiplier.

```

731 <WeightType>double</WeightType>
732 <Connections>
733 ...
734 <Connection In="RATEFUNC_BACKGROUND" Out="WC_POP">0.1</Connection>
735 ...
736 </Connections>
```

737 Many algorithms use the *DelayedConnection* weight type which requires three values to define each
 738 connection. The first is the number of incoming connections each neuron in the Out population receives
 739 from the In population. This number is effectively a weight and is multiplied by the output activity of the In
 740 population. For example, if the output firing rate of an In population is 10Hz and the number of incoming
 741 connections is set to 10, the effective average incoming spike rate to each neuron in the Out population
 742 will be 100 Hz. The second value is the post synaptic efficacy whose sign must match the type of the In
 743 population. If the Out population is an instance of MeshAlgorithm, the efficacy must also match one of the
 744 provided *.mat* files. The third value is the connection delay in seconds. The delay is implemented in the
 745 same way as the refractory period in the mesh and grid algorithms. The output activity of the In population
 746 is placed at the beginning of the queue and shifted towards the end of the queue over subsequent iterations.
 747 The input to the Out population is taken as the linear interpolation between the final two values in the
 748 queue.

Listing 19. A DelayedConnection with number of connections = 10, efficacy = 0.1, and delay of 1ms.

```

749 <WeightType>DelayedConnection</WeightType>
750 <Connections>
751 ...
752 <Connection In="RATEFUNC_BACKGROUND" Out="BURSTER">10 0.1 0.001</Connection>
753 ...
754 </Connections>
```

755 With the addition of GridAlgorithm, there was a need for a more flexible connection type which would
 756 allow custom parameters to be applied to each connection. When using the *CustomConnectionParameters*

757 weight type, the key-value attributes of the connections are passed as strings to the C++ implementation.
 758 By default, custom connections require the same three values as *DelayedConnection*: *num_connections*,
 759 *efficacy*, and *delay*. *CustomConnectionParameters* can therefore be used with mesh algorithm nodes as
 760 well as grid algorithm nodes although MeshAlgorithm definitions must have the type attribute set to
 761 MeshAlgorithmCustom instead.

Listing 20. A MeshAlgorithmCustom definition for use with WeightType=CustomConnectionParameters and a Connection using the num_connections, efficacy, and delay attributes.

```
762 <WeightType>CustomConnectionParameters</WeightType>
763
764 <Algorithms>
765 ...
766 <Algorithm type="MeshAlgorithmCustom" name="ALG_ADEX" modelfile="adex.model" >
767   <TimeStep>0.001</TimeStep>
768   <MatrixFile>adex_0.05_0_0_0_.mat</MatrixFile>
769   <MatrixFile>adex_-0.05_0_0_0_.mat</MatrixFile>
770 </Algorithm>
771 ...
772 </Algorithms>
773
774
775 <Connections>
776 ...
777 <Connection In="ALG_ADEX" Out="RG_E" num_connections="1" efficacy="0.05" delay="0.0"/>
778 ...
779 </Connections>
```

780 Other combinations of attributes for connections using CustomConnectionParameters are available for
 781 use with specific specialisations of the grid algorithm which are discussed in section 4 of the supplemen-
 782 tary material. Any number of attributes are permitted but they will only be used if there is an algorithm
 783 specialisation implemented in the MIIND code base.

784 4.4 SimulationRunParameter

785 The *<SimulationRunParameter>* block contains parameter settings for the simulation as a whole. The
 786 sub-elements listed in Table 5 are required for a full definition. Although most of the sub-elements are
 787 self explanatory, *t_step* has the limitation that it must match or be an integer multiple of all time steps
 788 defined by any MeshAlgorithm and GridAlgorithm instances. *master_steps* is used only for the GPGPU
 789 implementation of MIIND (section 5). It allows the user to set the number of Euler iterations per time step to
 790 solve the master equation. By default, the value is 10. However, to improve accuracy or to avoid blow-up in
 791 the case where the time step is too large or the local dynamics are unstable, *master_steps* should be increased.
 792

793 4.5 Reporting

794 The *<Reporting>* block is used to describe how output is displayed and recorded from the simulation.
 795 There are three ways to record output from the simulation: Density, Rate, and Display. The *<Rate>*
 796 element takes the node *name* and *t_interval* as attributes and creates a single file in the output directory.
 797 *t_interval* must be greater than or equal to the simulation time step. At each *t_interval* of the simulation, the
 798 output activity of the population is recorded on a new line of the generated file. Although the element is
 799 called “Rate”, if average membrane potential has been chosen as the activity of this population, this is what

801 will be recorded here. *<Density>* is used to record the full probability density of the given population node.
 802 As density is only relevant for the population density technique, it can only be recorded from nodes which
 803 instantiate the mesh or grid algorithm types. The attributes are the node *name*, *t_start*, *t_end*, and *t_interval*
 804 which define the simulation times to start and end recording the density at the given interval. A file which
 805 holds the probability mass values for each cell in the mesh or grid will be created in the output directory
 806 for each *t_interval* between *t_start* and *t_end*. Finally, the *<Display>* element can be used to observe the
 807 evolution of the probability density function as the simulation is running. If a *Display* element is added in
 808 the XML file for a specific node, when the simulation is run, a graphical window will open and display the
 809 probability density for each time step. Again, display is only applicable to algorithms involving densities.
 810 Enabling the display can significantly slow the simulation down. However, it is useful for debugging the
 811 simulation and furthermore, each displayed frame is stored in the output directory so that a movie can be
 812 made of the node's behaviour. How to generate this movie is discussed later in section 7.1.

Listing 21. A set of reporting definitions to record the probability densities and rates of two populations, S and D. The densities will also be displayed during simulation.

```
813 <Reporting>
814 ...
815   <Density node="S" t_start="0.0" t_end="6.0" t_interval="0.01" />
816   <Density node="D" t_start="0.5" t_end="1.5" t_interval="0.001" />
817   <Display node="S" />
818   <Display node="D" />
819   <Rate node="S" t_interval="0.0001" />
820   <Rate node="D" t_interval="0.0001" />
821 ...
822 </Reporting>
```

823 4.6 Variables

824 The *<Simulation>* element can contain multiple *<Variable>* sub-elements each with a unique name
 825 and value. Variables are provided for the convenience of the user and can replace any values in the XML
 826 file. For example, a variable named *TIME_END* can be defined to replace the value in the *t_end* element of
 827 the *SimulationRunParameter* block. When the simulation is run, the value of *t_end* will be replaced with
 828 the default value provided in the Variable definition. Using variables makes it easy to perform parameter
 829 sweeps where the same simulation is run multiple times and only the variable's value is changed. How
 830 parameter sweeps are performed is covered in the supplementary material section 8. All values in a MIIND
 831 XML script can be set with a variable name. The type of the Variable is implicit and an error will be thrown
 832 if, say, a non-numerical value is passed to the *tau_refractive* attribute of a *MeshAlgorithm* object.

Listing 22. A Variable definition. *TIME_END* has a default value of 18.0 and is used in the *t_end* parameter definition.

```
834 <Variable Name='TIME_END'>18.0</Variable>
835 ...
836 <t_end>TIME_END</t_end>
```

5 MIIND ON THE GPU

837 The population density techniques of the mesh and grid algorithms rely on multiple applications of the
 838 transition matrix which can be performed on each cell in parallel. This makes the algorithms prime
 839 candidates for parallelisation on the graphics card. In the CPU versions, the probability mass is stored

840 in separate arrays, one for each population/node in the simulation. For the GPGPU version, these are
 841 concatenated into one large probability mass vector so all cells in all populations can be processed in parallel.
 842 From the user's perspective, switching between CPU and GPU implementations is trivial. In the XML file
 843 for a simulation which uses MeshAlgorithm or GridAlgoirthm, to switch to the vectorised GPU version, the
 844 Algorithm types must be changed to MeshAlgorithmGroup and GridAlgorithmGroup. All other attributes
 845 remain the same. Only MeshAlgorithmGroup, GridAlgorithmGroup, and RateFunctor/RateAlgorithm
 846 types can be used for a vectorised simulation. When running a MIIND simulation containing a group
 847 algorithm from a Python script, instead of importing *miind.miindsim*, *miind.miindsimv* should be used. The
 848 Python module *miind.run* is agnostic to the use of group algorithms so can be used as shown previously.

Listing 23. A MeshAlgorithmGroup definition is identical to a MeshAlgorithm definition except for the type.

```
849 <Algorithm type="MeshAlgorithmGroup" name="ALG_ADEX" modelfile="adex.model" >
850   <TimeStep>0.001</TimeStep>
851   <MatrixFile>adex_0.05_0_0_.mat</MatrixFile>
852   <MatrixFile>adex_-0.05_0_0_.mat</MatrixFile>
853 </Algorithm>
854 <Algorithm type="GridAlgorithmGroup" name="OSC" modelfile="fn.model" tau_refractive="0.0" transformfile=
855   ↪ "fn_0_0_0_0_.tmat" start_v="-1.0" start_w="-0.3" ratemethod="AvgV">
856 <TimeStep>0.00001</TimeStep>
857 </Algorithm>
```

858 The GPGPU implementation uses the Euler method to solve the master process during each iteration. It
 859 is, therefore, susceptible to blow-up if the time step is large or if the local dynamics of the model are stiff.
 860 The user has the option to set the number of euler steps taken each iteration using the *master_steps* value of
 861 the SimulationRunParameter block in the XML file. A higher value reduces the likelihood of blow-up but
 862 increases the simulation time.

863

864 In order to run the vectorised simulations, MIIND must be running on a CUDA enabled machine and have
 865 CUDA enabled in the installation (CUDA is supported in the Windows and Linux python installations).
 866 Section 3 in the supplementary material goes into greater detail about the systems architecture differences
 867 between the CPU and GPU versions of the MIIND code. Using the “Group” algorithms is recommended if
 868 possible as it provides a significant performance increase. Benchmarking details for MIIND compared to
 869 direct simulation are available in De Kamps et al. (2019).

870

6 RUNNING A MIIND SIMULATION IN PYTHON

871 As demonstrated in the quick start guide, the command **python -m miind.run** takes a simulation XML file
 872 as a parameter and runs the simulation. A similar script may be written by the user to give more control
 873 over what happens during a simulation and how output activity is recorded and processed. It even allows
 874 MIIND simulations to be integrated into other Python applications such as the Virtual Brain (Sanz Leon
 875 et al., 2013) so the population density technique can be used to solve the behaviour of nodes in a brain-scale
 876 network (see section 9). To run a MIIND simulation in a Python script, the module *miind.miindsim* must be
 877 imported (or *miind.miindsimv* if the simulation uses MeshAlgorithmGroup or GridAlgorithmGroup and
 878 therefore requires CUDA support). Listing 24 shows an example script which uses the following available
 879 functions to control the simulation.

880

Listing 24. A simple python script for running a MIIND simulation and plotting the results.

```

881 import matplotlib.pyplot as plt
882 import miind.miindsim as miind
883
884 miind.init(1, "lif.xml")
885
886 timestep = miind.getTimeStep()
887 simulation_length = miind.getSimulationLength()
888 print('Timestep from XML : {}'.format(timestep))
889 print('Sim time from XML : {}'.format(simulation_length))
890
891 miind.startSimulation()
892
893 constant_input = [2500]
894 activities = []
895 for i in range(int(simulation_length/timestep)):
896     activities.append(miind.evolveSingleStep(constant_input)[0])
897
898 miind.endSimulation()
899
900 plt.figure()
901 plt.plot(activities)
902 plt.title("Firing Rate.")
903
904 plt.show()

```

905 6.1 init(node_count,simulation_xml_file,...)

906 The *init* function should be called first once the MIIND library has been imported. This sets up the
 907 simulation ready to be started. The *node_count* parameter allows for multiple instantiations of the simulation
 908 to be run simultaneously. The Nodes, Connections, and Reporting blocks from the simulation file will be
 909 duplicated, effectively running the same model *node_count* times simultaneously in the same simulation.
 910 This functionality was included to allow the Virtual Brain to run the simulation defined in the XML file
 911 multiple times (see section 9). The *simulation_xml_file* parameter gives the name of the simulation xml file
 912 to be run. If the file has any variables defined, these are made available in Python as additional parameters
 913 to the *init* function. In this way, the use of XML variables can be used for parameter sweeps. All variables
 914 must be passed as strings. If a variable is not set in the call to *init*, the default value defined in the XML file
 915 will be used.

Listing 25. Calling init for a MIIND simulation lif.xml with the Variable SIM_TIME set to 0.4.

```
916 miind.init(1, "lif.xml", SIM_TIME="0.4")
```

917 6.2 getTimeStep() and getSimulationLength()

918 Once *init* has been called, the functions *getTimeStep* and *getSimulationLength* can be used to extract the
 919 time step and simulation length in seconds from the simulation respectively. The Python script controls
 920 when each iteration of the MIIND simulation is called and so it needs to know the total number of iterations
 921 to make. Furthermore, it can be useful for integration with other systems to know these values.

923 **6.3 startSimulation()**

924 *startSimulation* indicates in the Python script that the simulation should be initialised ready for the
925 simulation loop to be called.

926 **927 6.4 evolveSingleStep(input)**

928 By calling *evolveSingleStep* in the Python script, the MIIND simulation will move forward one time step.
929 This function takes a list of numbers as a parameter. The list corresponds to inputs to the population nodes
930 in the MIIND simulation. In this way, the user may control the behaviour of the simulation from the Python
931 script during the simulation. The *evolveSingleStep* function also returns a list of numbers which are the
932 output activities of the population nodes. Section 6.6 provides more information about how to use the input
933 and output of this function. *evolveSingleStep* should be called in a loop which will run the same number of
934 iterations as would be expected if the XML file were run in MIIND directly, that is, the simulation length
935 divided by the time step.

936 **937 6.5 endSimulation()**

938 It is good practice to call *endSimulation* once all iterations of the simulation have been performed. This
939 allows MIIND to clean up and to print the performance statistics to the console.

940 **941 6.6 Additional XML Code for Python Support**

942 Although it is still possible to use *RateFunctor* or *RateAlgorithm* to set input rates to populations in a
943 Python MIIND simulation, *evolveSingleStep()* provides a means to pass the input rates as a parameter so
944 that more complex input patterns can be used. In order to indicate that a population will receive input
945 externally from the Python script (via the list input to *evolveSingleStep()*) a special connection type must
946 be defined in the *<Connections>* section of the XML.

Listing 26. Special connection types for use in Python.

```
947 <Connections>
948 ...
949 <IncomingConnection Node="E">1 0.01 0</IncomingConnection>
950 <OutgoingConnection Node="E"/>
951 ...
952 </Connections>
```

953 Listing 26 defines an input to node E which will be interpreted as a *DelayedConnection* with the number
954 of connections equal to 1 and a post synaptic efficacy of 0.01. No delay is defined here although it is
955 permitted. *OutgoingConnections* are used to declare which nodes in the population network will pass their
956 activity back to the Python script after each iteration. If the two connections in the listing are the only
957 instances of *IncomingConnection* and *OutgoingConnection*, then the *evolveSingleStep* function will expect
958 as a parameter, a list with one numeric value to represent the incoming rate to node E. *evolveSingleStep*
959 will return a list with a single numeric value representing the activity of node E. In cases where there are
960 more than one *IncomingConnection*, the order of values in the Python list parameter to *evolveSingleStep* is
961 the same as the order of *IncomingConnections* defined in the XML. Similarly with *OutgoingConnections*,
962 the order of the list of activities returned from *evolveSingleStep* is the same as the order of declaration in
963 the XML file.

7 USING THE CLI TO QUICKLY VIEW RESULTS

964 Once a simulation has been run, either using *miind.run* or from a user written Python script, the
965 *miind.miindio* CLI can be used to quickly plot the recorded results. As mentioned, the commands used
966 in *miindio* are based on the module *miind.miind_api* and are reproducible in a Python script. However, it
967 can be convenient to be able to run them directly from the command line to aid fast prototyping and bug
968 fixing of models and simulations. The following section lists some common commands in the CLI and
969 their usage. The accompanying files for this example are in the *examples/cli_plots* directory. The following
970 command starts the CLI and presets the user with a prompt:

Listing 27. Run the CLI.

```
971 $ python -m miind.miindio
```

972 When *miind.miindio* is called for the first time in a working directory, the user must identify the XML file
973 which will describe the current working simulation. MIIND stores a reference to this file in a settings file in
974 the working directory so that all subsequent commands will reference this simulation. Even if *miind.miindio*
975 is quit and restarted, the current working simulation will be used as the context for commands until a new
976 current working simulation is defined or if it is called in a different directory. The user can set the current
977 working simulation with the **sim** command.

978

Listing 28. Load a simulation file in the CLI.

```
979 > sim example.xml
```

980 Calling **sim** without a parameter will list information about the current working simulation such as the
981 output directory, XML file name and provide a list of the defined variables and nodes.

982

983 During the simulation, MIIND generates output files according to the requirements of the *<Recording>*
984 object of the XML file which could include the average firing rate of population nodes or their densities at
985 each time interval. The average firing rate can be plotted from the CLI using the **rate** command followed by
986 the name of the population node. To be reminded of the node names, the user can call **sim** or **rate** without
987 parameters.

988

Listing 29. Plot the rate of population POP1 in the CLI.

```
989 > rate POP1
```

990 Even while a simulation is running, calling **rate** in the CLI will plot the recorded activity up to the latest
991 simulated time point. This is useful to keep an eye on the simulation as it progresses without waiting for
992 completion. An example of the plots produced by **rate** is shown in Fig. 11A.

993 For populations using the grid or mesh algorithms, the user can call the **plot-density** command with
994 parameters identifying the required node name and simulation time.

995

Listing 30. Plot the probability density of population POP1 at time 0.42s in the CLI.

```
996 > plot-density POP1 0.42
```

997 This command renders the mesh or grid and its population density at the given simulation time. When
998 reading the simulation time parameter in the command, MIIND expects the time to be an integer multiple

999 of the time step and to be expressed up to its least significant figure (for example, 0.1 instead of 0.10).
1000 Again, this command can be run during a simulation providing the time has been simulated. An example of
1001 a density plot is shown in Fig. 11B.
1002

1003 Similar to **plot-density**, **plot-marginals** can be used to display the marginal densities of a given popula-
1004 tion at a given time. Both marginals are plotted next to each other. The details of how marginal densities are
1005 calculated are explained in the supplementary material section 5. Fig. 11C shows an example of a marginal
1006 density plot.
1007

Listing 31. Plot the marginal distributions of population POP1 at time 0.42s in the CLI.

1008 > plot-marginals POP1 0.42

1009 7.1 Generate a Density Movie

1010 If, in the XML file *<Recording>* section, the *<Display>* element is added for a given population, the
1011 output directory will be populated with still images of density plots at each time step. Once the simulation
1012 is complete, calling **generate-density-movie** in the CLI will produce an MP4 movie file made from the
1013 still images. The parameters are the node name followed by the size of the square video frame in pixels.
1014 The third parameter is the desired time to display each image (every time step of the simulation) in seconds.
1015 If the video should be the same length as the simulation time, then this parameter should match the time
1016 step of the simulation. By changing the value, the video time can be altered. For example, if the parameter
1017 is set to 0.01 for a simulation with time step 0.001, then the video length will be 10 times the length of the
1018 simulation. Finally, a name for the video file must be given.

Listing 32. Generate a movie from the display images of population POP1 with a size of 512 pixels at a
simulation replay time step of 0.1s.

1019 > generate-density-movie POP1 512 0.1 pop1_mov

1020 The movie file will be created in the working directory of the simulation. A movie of the marginal density
1021 plots can also be created using the **generate-marginal-movie** command which takes the same parameters.
1022 As each marginal plot must be generated from the density output, this takes a considerably longer time
1023 than for the density movie.

Listing 33. Generate a marginals movie from the density files of population POP1 with a size of 512
pixels at a simulation replay time step of 0.1s.

1024 > generate-marginal-movie POP1 512 0.1 pop1_marginal_mov

8 DESCRIPTION OF MIIND'S ARCHITECTURE AND FUNCTIONALITY

1025 The main architectural concerns in MIIND relate to the two C++ libraries, MPILib and TwoDLib. MPILib
1026 is responsible for instantiating and running the simulation. TwoDLib contains the CPU implementations of
1027 the grid and mesh algorithms. It is also responsible for generating transition matrices. Of the remaining
1028 libraries, GeomLib contains a population density technique implementation of neuron models with one
1029 time dependent variable, although it is also possible and indeed preferable to use the TwoDLib code for
1030 one dimensional models. EPFLlib and NumtoolsLib contain helper classes and type definitions. Fig. 12
1031 shows a reduced UML diagram of the MIIND C++ architecture. The aim of this section is to give a brief
1032 overview of the C++ MIIND code as a starting point for developers. The CUDA implementation of MIIND
1033 is similar in structure to the CPU solution and is available in the CudaTwoDLib and MiindLib libraries. A

1034 description of the differences is given in section 3 of the supplementary material.

1035 1036 8.1 MPILib

1037 The MPINetwork class in MPILib represents a simulation as a whole and is instantiated in the *init* function
1038 of the SimulationParserCPU class which is a specialisation of MiindTvbModelAbstract. *init* is called from
1039 the Python module and, as the name suggests, MiindTvbModelAbstract was originally written with the aim
1040 of Python integration into TVB. MPINetwork exposes member functions for building a network of nodes
1041 where each node is an instance of a neuron population which can be connected together so that the output
1042 activity from one population is input to another. The class also contains all of the simulation parameters
1043 such as the simulation length and time step. Finally, the MPINetwork class exposes a function to run the
1044 simulation in its entirety or take a single evolve step for use in an external control loop.

1045

1046 Each node in the population network is represented by an instance of the MPINode class. A node
1047 has a name and an ID which is used to uniquely identify it in the simulation. A node also contains an
1048 implementation of AlgorithmInterface performing the integration technique required for this population
1049 (for example, GridAlgorithm or MeshAlgorithm). The *NodeType* describes whether a population should be
1050 thought of as excitatory or inhibitory. As discussed earlier, MIIND performs a validation check that the
1051 synaptic efficacy from a node is positive or negative respectively (or neutral). During each iteration, each
1052 node is responsible for consolidating the activity of all input connections, calling the integration step in the
1053 AlgorithmInterface implementation, and reporting the density and output activity (the average firing rate or
1054 membrane potential).

1055

1056 In MPILib, a number of implementations of AlgorithmInterface are defined which can be instantiated
1057 in a node. Implementations of AlgorithmInterface are responsible for the lion’s share of the computation
1058 in MIIND as this is where the integration of the model is performed. The interface is extremely simple,
1059 providing a function to set parameters, an optional function for a preamble before each iteration, and
1060 the *evolveNodeState* function to be called every time step. GridAlgorithm and MeshAlgorithm are imple-
1061 ments of this interface defined in TwoDLib. MPILib and GeomLib hold the implementations of the
1062 remaining algorithms available to the user which were discussed in section 4. Finally, the weight types,
1063 DelayedConnection and CustomConnectionParameters are also defined in MPILib. All classes are C++
1064 templates which take the weight type as a parameter to avoid code duplication and to enforce that only
1065 algorithms with the same weight type can be used together.

1066 1067 8.2 TwoDLib

1068 As with the population models in MPILib and GeomLib, GridAlgorithm and MeshAlgorithm are imple-
1069 ments of the AlgorithmInterface. We will focus here on the grid algorithm implementation although
1070 the mesh algorithm uses the same structures or specialisations of those structures to perform similar tasks
1071 as set out in section 3. GridAlgorithm is supported by two important classes. **Ode2DSys** transfers
1072 probability mass according to the reset mapping of the *.model* file and calculates the average firing rate of
1073 the population. In MeshAlgorithm, Ode2DSys also performs the pointer update for shifting probability
1074 mass down the strips of the mesh. **MasterGrid** is responsible for solving the Poisson master equation using
1075 a transition matrix calculated at simulation time based on the desired efficacy and grid cell size. For each
1076 iteration, the function *evolveNodeState* is called which performs the main steps of the population density

1077 algorithm.

1078

1079 First, in GridAlgorithm, the deterministic dynamics are solved by applying the pre-generated transition
1080 matrix once. The second step is a call to *Ode2DSys*.*RedistributeProbability()* to perform any reset
1081 mappings for probability mass which appeared in the threshold cells last iteration. This step is useful for
1082 neuron models, such as leaky integrate and fire, which contain an instruction to reset one or more variables
1083 to a different value upon reaching a threshold.

1084

1085 The third step calls on the MasterGrid class to solve the master equation for the incoming Poisson spike
1086 rates from every incident node. MasterGrid begins with the current state of the probability mass distribution
1087 across the grid, that is, the probability mass values of each cell in the grid. As described in section 2, every
1088 cell has the same relative transition of probability mass due to a single incoming spike. For the whole
1089 grid, this single transition is duplicated into a transition matrix which can be applied to the full probability
1090 mass vector. Because there are at most two cells into which probability mass is transferred, this matrix
1091 is extremely sparse and can be stored efficiently in a compressed sparse row (CSR) matrix. In the mesh
1092 algorithm, this matrix is loaded from the .mat file.

1093

1094 MeshAlgorithm requires a fourth step to transfer probability mass from the ends of strips to stationary
1095 cells subject to a reversal mapping generated during the pre-processing phase. This is discussed in the
1096 supplementary material section 6.

1097

1098 Finally, SimulationParserCPU is an extension of the MiindTvbModelAbstract class used to parse the
1099 simulation XML file and instantiate an MPINetwork object with the appropriate nodes and connections. Its
1100 extensions of the functions declared in MiindTvbModelAbstract are exposed to the Python module to be
1101 called from a Python script.

9 DISCUSSION

1102 MIIND fulfills a need for insight into neural behaviour at mesoscopic scales.

1103 The MIIND population density technique allows researchers to simulate population level behaviour by
1104 defining the behaviour of the underlying neurons. This is in contrast to many rate based models which
1105 describe the population behaviour directly. An example of how population behaviour can differ from the
1106 underlying neuron model can be seen in the behaviour of a population of bursting neurons such as the
1107 Izhikevich simple model. A single Izhikevich neuron with a constant input current or input spike rate
1108 oscillates between a bursting period of repeated firing and a quiescent period of no firing. The average
1109 behaviour of a population of Izhikevich neurons is different. Initially, all neurons are synchronised, they
1110 burst and quiesce at the same time producing an oscillatory pattern of average firing rate in the population.
1111 However, due to the random nature of Poisson input spikes, the neurons de-synchronise over time and the
1112 average firing rate of the whole population damps to a constant value because only a subset of neurons
1113 are bursting at any one time. Fig. 11A shows the damping of the output firing rate oscillations and the
1114 ‘desynchronised’ density of a population of Izhikevich simple neurons.

1115

1116 TVB Integration

1117 The Virtual Brain (Sanz Leon et al., 2013) and MIIND are both systems which facilitate the development
1118 of neural mass or mean field population models with explicit descriptions of how multiple populations are
1119 connected. Using these systems, the complex dynamics arising from the interaction of populations can be
1120 studied.

1121 TVB provides a framework to describe a network of nodes (the connectivity) which, while it can be abstract,
1122 generally represents regions of the human or primate brain. Connections between nodes represent white
1123 matter tracts which transfer signals from one node to the next based on length and propagation speed. TVB
1124 also allows the description of “coupling” functions which modulate these signals as they pass from one
1125 node to another. Typically, the number of nodes is in the order of 100 or so. However, TVB also allows for
1126 the definition of a “surface” which can be associated with 10s of thousands of nodes to simulate output
1127 from common medical recording techniques such as EEG and BOLD fMRI. TVB has impressive clinical
1128 relevance as well as supporting more theoretical neuroscience research. Users can build simulations using
1129 the graphical user interface or directly using the Python source code.
1130

1131 While MIIND and TVB have many functional similarities, both have differing strengths with respect to
1132 the underlying simulation techniques and surrounding infrastructure. It was therefore clear that integrating
1133 the smaller system, MIIND, into the more developed infrastructure of TVB might yield benefits from both.
1134

1135 Although it is possible to model delayed connections and synaptic dynamics between populations in
1136 MIIND, TVB provides a comprehensive method of defining such structures and behaviours through the
1137 connectivity network and coupling functions. Some users of MIIND may find it useful and appropriate to
1138 house their simulations in such a structure.
1139

1140 TVB uses a number of model classes to describe the behaviour of the nodes in a network. When the
1141 simulation is run, an instantiation of a specified model class takes the signals which have passed through
1142 the network to arrive at each node and integrates forward by one time step (depending on the integration
1143 method). In order to use MIIND nodes in TVB, a specialised model class was created to import the MIIND
1144 Python library, instantiate it, then make a call to *evolveSingleStep()* in place of the integration function. The
1145 inputs and outputs of *evolveSingleStep()* are treated by TVB as any other model. As the MIIND Python
1146 library takes a simulation file name as a parameter to its *init* function, a single additional model class is all
1147 that is required to expose any MIIND simulation to TVB. Fig. 13 shows the results from a simulation of
1148 the TVB default whole-brain connectivity with populations of Izhikevich simple neurons in MIIND. The
1149 script and simulation files are available in the *examples/miind_tvb* directory of the MIIND repository. Both
1150 TVB and MIIND must be installed to sucessfully run the example.
1151

1152 Reasoning about probability density instead of populations of individual neurons 1153 simplifies output analysis.

1154 The output firing rate or membrane potential of a MIIND population which uses the the mesh algorithm
1155 or grid algorithm is devoid of any variation which you would see from a population of individual neurons.
1156 This is because the effect of Poisson generated input spike trains is applied to a probability density function,
1157 effectively an infinite population of neurons. Spike train inputs to a finite population of neurons produces
1158 variation in how individual neurons move through state space resulting in noisy output rates at the popula-
1159 tion level. While this can be mitigated using a larger number of neurons, the use of smoothing techniques,

1160 or curve fitting, MIIND requires none of these methods to produce an output which is immediately clear to
1161 interpret. For example, MIIND was used to build and simulate a spinal circuit model using populations
1162 of integrate and fire neurons (York et al., 2019). The average firing rates of the populations were used to
1163 compare patterns of activity with results from an EMG experiment. As the patterns to be observed were
1164 on the order of seconds, there was no need to capture faster variation in activity from the simulation and
1165 indeed, a direct simulation would have produced output which may have obscured these patterns.
1166

1167 MIIND has also been used to simulate central pattern generator models which rely on mutually inhibiting
1168 populations of bursting neurons. The interaction of the two populations significantly influences their sub-
1169 threshold dynamics. In particular, it can be difficult to identify the dynamics responsible for the swapping
1170 of states from bursting to quiescent (escape or release). Observing the changing probability density function
1171 during the simulation makes it very clear how the two populations are behaving.
1172

Handling Noise

1173 A major benefit of MIIND's population density technique is the ability to observe the effect of noise on a
1174 population, and to manipulate noise in an intuitive way. For a given simulation, the Poisson distributed
1175 input to a population causes a spread of probability mass across the state space as some neurons receive
1176 many spikes, and some receive fewer. It is explained in de Kamps (2013) how the Poisson input causes a
1177 mean increase in membrane potential equal to the product of the post synaptic efficacy, h , and the average
1178 input rate, ν . It causes a variance equal to νh^2 . h and ν can therefore be set such that the mean remains the
1179 same but the variance changes to observe the effect of noise on the population.
1180

1181

1182 Another simple way to increase the variance of the population is to introduce two additional inputs with
1183 equal rates and opposite post-synaptic efficacies. Again, the mean increase caused by the input remains
1184 unchanged but the variance can be increased significantly and this requires only a small change to the XML
1185 simulation file.
1186

A model agnostic system at the population level makes prototyping quick and intuitive.

1187 Because MIIND provides insight of how a neuron model produces behaviour at the population level, it is
1188 beneficial that the grid algorithm enables the user to quickly reproduce the *.model* and *.tmat* files if the
1189 underlying neuron model needs to be changed. An example of this can be observed in a half-centre oscillator
1190 made of a pair of mutually inhibiting populations of bursting neurons. The frequency of oscillation can be
1191 made dependent or independent of the input spike rate by including a limit on the slow excitability variable
1192 of the underlying neuron model. To make this change, the user can alter the neuron model then rebuild the
1193 *.model* and *.tmat* file and no change to the population level network is required.
1194

DipDE

1195 DipDE (DiPDE, 2015; Iyer et al., 2013) is an alternative implementation of the population density
1196 technique for one dimensional neuron models. It does not employ the “mesh” discretisation method used
1197 in the MIIND mesh algorithm and has primarily been used with populations of leaky integrate and fire
1198 neurons. DiPDE can be used to simulate the Potjans-Diesmann microcircuit model (Cain et al., 2016)
1199 which shows good agreement with MIIND (Fig. 5). MIIND is a much larger application than DiPDE
1200 because it allows users to design their own underlying neuron models for each population using either the
1202

1203 mesh or grid algorithms.

1204

1205 Future Work

1206 A limitation on the MIIND population density technique is that a maximum of two time-dependent
1207 variables can be used to describe the underlying neuron model of each population. In the mesh algorithm,
1208 for higher dimensions, mesh building would need to be automated but this is not a trivial problem to solve.
1209 The grid algorithm, however, is entirely automated and work has been done to extend MIIND for 3D
1210 neuron models. Fig. 14 shows the 3D density plot of a population of Hindmarsh-Rose neurons in MIIND.
1211 The technique used to generate the 2D transition matrices outlined in section 2 extends to N dimensions so
1212 there is theoretically no limit to the dimensionality of the underlying neuron model in the grid algorithm.
1213 However, both the grid algorithm and mesh algorithm suffer from “the curse of dimensionality” such that
1214 with each additional variable, the number of cells to cover the state space increases to the point where the
1215 memory and processing requirements are too high. Luckily, a great number of neuron behaviours can be
1216 captured with only two or three time-dependent variables with appropriate approximations.

1217

1218 Large networks can be built up quickly in MIIND. To add a node to a simulation file requires just a
1219 single line. Integrating the node into the rest of the network with requisite connections is equally convenient.
1220 As mentioned, the Potjans-Diesmann model has been implemented as a single cortical column but this is
1221 by no means the limit of the size of network which can be built. It is feasible that a patch of cortex made of
1222 perhaps hundreds of cortical columns can be simulated efficiently in MIIND. The benefit of such a network
1223 would be to demonstrate how cortical columns interact together under different connectivity regimes and
1224 inputs as well as providing the ability to quickly and easily “swap out” the underlying neuron model of
1225 each population. Typically, LIF is used but adaptive integrate and fire would be a closer approximation to
1226 pyramidal neurons in cortex.

1227

1228 Conclusion

1229 We have reintroduced MIIND’s population density techniques for simulating populations of neurons
1230 and given a full account of the features available to users. While the mesh algorithm was developed some
1231 time ago, the grid algorithm which was added to MIIND recently has precipitated a more accessible, user
1232 friendly software package. We hope that the explanations given here along with a lower technical barrier to
1233 entry will encourage researchers to make use of the tool.

CONFLICT OF INTEREST STATEMENT

1234 The authors declare that the research was conducted in the absence of any commercial or financial
1235 relationships that could be construed as a potential conflict of interest.

AUTHOR CONTRIBUTIONS

1236 HO and MdK contributed to the text of this article. YML, MEL, DS, and LD contributed to the development
1237 of the population density technique and MIIND software.

1238

FUNDING

1239 This project received funding from the European Union’s Horizon 2020 research and innovation programme
1240 under Grant Agreement No. 720270 (HBP SGA1) and Specific Grant Agreement No. 785907 (Human

1241 Brain Project SGA2) (MdK; YML). HO is funded by EPSRC. The funders had no role in study design,
1242 data collection and analysis, decision to publish, or preparation of the manuscript.

ACKNOWLEDGMENTS

1243 The authors wish to thank Frank van der Velde and Martin Perez-Guevara for their continued support of
1244 the MIIND project.

DATA AVAILABILITY STATEMENT

1245 The MIIND source code and installation packages are available as a github repository at <https://github.com/dekamps/miind>.
1246 MIIND can be installed for use in Python using “pip install miind” on many Linux, MacOS, and Windows
1247 machines with python versions ≥ 3.6 .
1249 Documentation is available at <https://miind.readthedocs.io/>.

REFERENCES

- 1250 Amit, D. J. and Brunel, N. (1997). Model of global spontaneous activity and local structured activity
1251 during delay periods in the cerebral cortex. *Cerebral cortex (New York, NY: 1991)* 7, 237–252
1252 Bower, J. M. and Beeman, D. (2012). *The book of GENESIS: exploring realistic neural models with the*
1253 *GEneral NEural SImulation System* (Springer Science & Business Media)
1254 Brette, R. and Gerstner, W. (2005). Adaptive exponential integrate-and-fire model as an effective description
1255 of neuronal activity. *Journal of neurophysiology* 94, 3637–3642
1256 Brunel, N. and Hakim, V. (1999). Fast global oscillations in networks of integrate-and-fire neurons with
1257 low firing rates. *Neural computation* 11, 1621–1671
1258 Cain, N., Iyer, R., Koch, C., and Mihalas, S. (2016). The computational properties of a simplified cortical
1259 column model. *PLoS computational biology* 12, e1005045
1260 Carlu, M., Chehab, O., Dalla Porta, L., Depannemaeker, D., Héricé, C., Jedynak, M., et al. (2020). A
1261 mean-field approach to the dynamics of networks of complex neurons, from nonlinear integrate-and-fire
1262 to hodgkin-huxley models. *Journal of neurophysiology* 123, 1042–1051
1263 D’Angelo, E., Antonietti, A., Casali, S., Casellato, C., Garrido, J. A., Luque, N. R., et al. (2016). Modeling
1264 the cerebellar microcircuit: new strategies for a long-standing issue. *Frontiers in cellular neuroscience*
1265 10, 176
1266 de Kamps, M. (2013). A generic approach to solving jump diffusion equations with applications to neural
1267 populations. *arXiv preprint arXiv:1309.1654*
1268 De Kamps, M., Lepperød, M., and Lai, Y. M. (2019). Computational geometry for modeling neural
1269 populations: From visualization to simulation. *PLoS computational biology* 15, e1006729
1270 De Kamps, M., Lepperød, M., Lai, Y. M., and Osborne, H. (2020). *MIIND : Multiple Instantiations of*
1271 *Interacting Neural Dynamics [Internet]. Available from: http://miind.sourceforge.net.*
1272 DiPDE (2015). *Website: © 2015 Allen Institute for Brain Science. DiPDE Simulator [Internet]. Available*
1273 *from: https://github.com/AllenInstitute/dipde.*
1274 El Boustani, S. and Destexhe, A. (2009). A master equation formalism for macroscopic modeling of
1275 asynchronous irregular activity states. *Neural computation* 21, 46–100
1276 FitzHugh, R. (1961). Impulses and physiological states in theoretical models of nerve membrane.
1277 *Biophysical journal* 1, 445

- 1278 Fourcaud-Trocmé, N., Hansel, D., Van Vreeswijk, C., and Brunel, N. (2003). How spike generation
1279 mechanisms determine the neuronal response to fluctuating inputs. *Journal of Neuroscience* 23, 11628–
1280 11640
- 1281 Furber, S., Galluppi, F., Temple, S., and Plana, L. (2014). The spinnaker project. *IEEE. Proceedings* 102,
1282 652–665. doi:10.1109/JPROC.2014.2304638
- 1283 Gerstner, W. (1998). *Spiking neurons*. Tech. rep., MIT-press
- 1284 Gewaltig, M.-O. and Diesmann, M. (2007). Nest (neural simulation tool). *Scholarpedia* 2, 1430
- 1285 Hindmarsh, J. L. and Rose, R. (1984). A model of neuronal bursting using three coupled first order
1286 differential equations. *Proceedings of the Royal society of London. Series B. Biological sciences* 221,
1287 87–102
- 1288 Hines, M. L. and Carnevale, N. T. (2001). Neuron: a tool for neuroscientists. *The neuroscientist* 7, 123–135
- 1289 Iyer, R., Menon, V., Buice, M., Koch, C., and Mihalas, S. (2013). The influence of synaptic weight
1290 distribution on neuronal population dynamics. *PLoS Comput Biol* 9, e1003248
- 1291 Izhikevich, E. M. (2003). Simple model of spiking neurons. *IEEE Transactions on neural networks* 14,
1292 1569–1572
- 1293 Izhikevich, E. M. (2007). *Dynamical systems in neuroscience* (MIT press)
- 1294 Jirsa, V. K., Stacey, W. C., Quilichini, P. P., Ivanov, A. I., and Bernard, C. (2014). On the nature of seizure
1295 dynamics. *Brain* 137, 2210–2230
- 1296 Kamps, M. d. (2003). A simple and stable numerical solution for the population density equation. *Neural
1297 computation* 15, 2129–2146
- 1298 Knight, B. W. (1972). Dynamics of encoding in a population of neurons. *The Journal of general physiology*
1299 59, 734–766
- 1300 Knight, B. W., Manin, D., and Sirovich, L. (1996). Dynamical models of interacting neuron populations in
1301 visual cortex. *Robot Cybern* 54, 4–8
- 1302 Lai, Y. M. and de Kamps, M. (2017). Population density equations for stochastic processes with memory
1303 kernels. *Physical Review E* 95, 062125
- 1304 Mattia, M. and Del Giudice, P. (2002). Population dynamics of interacting spiking neurons. *Physical
1305 Review E* 66, 051917
- 1306 Mattia, M. and Del Giudice, P. (2004). Finite-size dynamics of inhibitory and excitatory interacting spiking
1307 neurons. *Physical Review E* 70, 052903
- 1308 Montbrió, E., Pazó, D., and Roxin, A. (2015). Macroscopic description for networks of spiking neurons.
1309 *Physical Review X* 5, 021028
- 1310 Nagumo, J., Arimoto, S., and Yoshizawa, S. (1962). An active pulse transmission line simulating nerve
1311 axon. *Proceedings of the IRE* 50, 2061–2070
- 1312 Nykamp, D. Q. and Tranchina, D. (2000). A population density approach that facilitates large-scale
1313 modeling of neural networks: Analysis and an application to orientation tuning. *Journal of computational
1314 neuroscience* 8, 19–50
- 1315 Omurtag, A., Knight, B. W., and Sirovich, L. (2000). On the simulation of large populations of neurons.
1316 *Journal of computational neuroscience* 8, 51–63
- 1317 Potjans, T. C. and Diesmann, M. (2014). The cell-type specific cortical microcircuit: relating structure and
1318 activity in a full-scale spiking network model. *Cerebral cortex* 24, 785–806
- 1319 Proix, T., Bartolomei, F., Guye, M., and Jirsa, V. K. (2017). Individual brain structure and modelling
1320 predict seizure propagation. *Brain* 140, 641–654
- 1321 Sanz Leon, P., Knock, S. A., Woodman, M. M., Domide, L., Mersmann, J., McIntosh, A. R., et al. (2013).
1322 The virtual brain: a simulator of primate brain network dynamics. *Frontiers in neuroinformatics* 7, 10

- 1323 Traub, R. D., Contreras, D., Cunningham, M. O., Murray, H., LeBeau, F. E., Roopun, A., et al. (2005).
1324 Single-column thalamocortical network model exhibiting gamma oscillations, sleep spindles, and
1325 epileptogenic bursts. *Journal of neurophysiology* 93, 2194–2232
- 1326 Tsodyks, M. V. and Markram, H. (1997). The neural code between neocortical pyramidal neurons depends
1327 on neurotransmitter release probability. *Proceedings of the national academy of sciences* 94, 719–723
- 1328 Uhlenbeck, G. E. and Ornstein, L. S. (1930). On the theory of the brownian motion. *Physical review* 36,
1329 823
- 1330 Wilson, H. R. and Cowan, J. D. (1972). Excitatory and inhibitory interactions in localized populations of
1331 model neurons. *Biophysical journal* 12, 1–24
- 1332 Wilson, M. A., Bhalla, U. S., Uhley, J. D., and Bower, J. M. (1988). Genesis: a system for simulating
1333 neural networks
- 1334 York, G., Osborne, H., Sriya, P., Astill, S., De Kamps, M., and Chakrabarty, S. (2019). Muscles recruited
1335 during an isometric knee extension task is defined by proprioceptive feedback. *BioRxiv* , 802736

TABLES

Table 1. Parameters for the `grid_generate.generate` function.

Parameter Name	Notes
<code>func</code>	The underlying neuron model function.
<code>timestep</code>	The desired time step for the neuron model
<code>timescale</code>	A scale factor for the timescale of the underlying neuron model to convert the time step into seconds.
<code>tolerance</code>	An error tolerance for solving a single time step of the neuron model.
<code>basename</code>	The base name with which all output files will be named.
<code>threshold_v</code>	The spike threshold value for integrate and fire neuron models.
<code>reset_v</code>	The reset value for integrate and fire neuron models.
<code>reset_shift_h</code>	A value for increasing the second variable during reset for integrate and fire neuron models with some adaptive shift or similar function.
<code>grid_v_min</code>	The minimum value for the first dimension of the grid (usually membrane potential).
<code>grid_v_max</code>	The maximum value for the first dimension of the grid.
<code>grid_h_min</code>	The minimum value for the second dimension of the grid.
<code>grid_h_max</code>	The maximum value for the second dimension of the grid.
<code>grid_v_res</code>	The number of columns in the grid.
<code>grid_h_res</code>	The number of rows in the grid.
<code>efficacy_orientation</code>	The direction, ‘v’ or ‘h’, in which incoming spikes cause an instantaneous change.

Table 2. Parameters for the `generate-model` command in the CLI.

Parameter Name	Notes
<code>basename</code>	The shared name of the <code>.mesh</code> , <code>.stat</code> , <code>.rev</code> and generated <code>.model</code> files.
<code>reset</code>	The value (usually representing membrane potential) which probability mass will be transferred to having passed the threshold.
<code>threshold</code>	The value (usually representing membrane potential) beyond which probability mass will be transferred to the reset value.

Table 3. Parameters for the `generate-matrix` command in the CLI.

Parameter Name	Notes
<i>basename</i>	The shared name of the <code>.model</code> , <code>.fid</code> (if required), and generated <code>.mat</code> files.
<i>v_efficacy</i>	The efficacy value in the <i>v</i> (membrane potential) direction. If the parameter <i>h_efficacy</i> is used, this should be zero.
<i>points / precision</i>	For Monte Carlo, this gives the number of points per cell to use for approximating the transition matrix. For the geometric method, transitions are stored in the <code>.mat</code> file to the nearest $\frac{1}{precision}$
<i>h_efficacy</i>	The efficacy value in the <i>h</i> direction. If the parameter <i>v_efficacy</i> is used, this should be zero.
<i>reset-shift</i>	The shift in the <i>h</i> direction which neurons take when being reset.
<i>use_geometric</i>	A boolean flag set to “true” if the geometric method is used and “false” for Monte Carlo.

Table 4. Compatible weight types for each algorithm type defined in the simulation XML file.

Algorithm Name	double	DelayedConnection	CustomConnectionParameters
<i>RateAlgorithm</i>	✓	✓	✓
<i>MeshAlgorithm</i>		✓	
<i>MeshAlgorithmCustom</i>			✓
<i>GridAlgorithm</i>			✓
<i>GridJumpAlgorithm</i>			✓
<i>OUAlgorithm</i>		✓	✓
<i>WilsonCowanAlgorithm</i>	✓		
<i>RateFunctor</i>	✓	✓	✓

Table 5. The required sub-elements for the `SimulationRunParameter` section of the XML simulation file.

Element	Notes
<i>SimulationName</i>	The name of the simulation.
<i>t_end</i>	The simulation end time.
<i>t_step</i>	The time step of the simulation.
<i>name_log</i>	A file name for logging. The file is stored in the output directory of the simulation.
<i>master_steps</i>	The number of Euler iterations per time step used to solve the master equation in the GPGPU implementation.

FIGURES

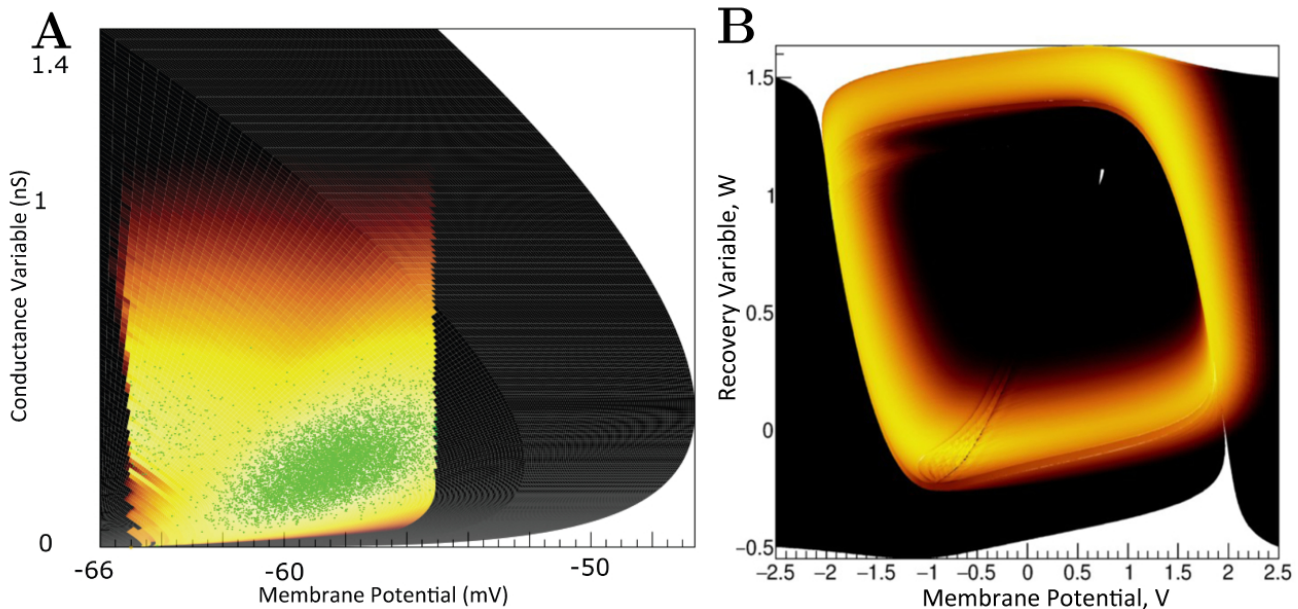


Figure 1. (A) The state space of a conductance based point model neuron. It is spanned by two variables: the membrane potential and a variable representing how open the channel is. This channel has an equilibrium potential that is positive. The green dots represent the state of individual neurons in a population. They are the result of the direct simulation of a group of neurons. MIIND, however, produces the heat plot representing a density which predicts where neurons in the population are likely to be: most likely in the white areas, least likely in the red areas and not at all in the black areas. The sharp vertical cut of the coloured area at -55mV represents the threshold at which neurons are removed from state space. They are subsequently inserted at the reset potential, at their original conductance state value. (B) The state space of a Fitzhugh-Nagumo neuron model. The axes have arbitrary units for variables V and W . There is no threshold-reset mechanism and the density follows a limit cycle. After a certain amount of simulation time, neurons can be found at all points along the limit cycle as shown here by a consistently high brightness.

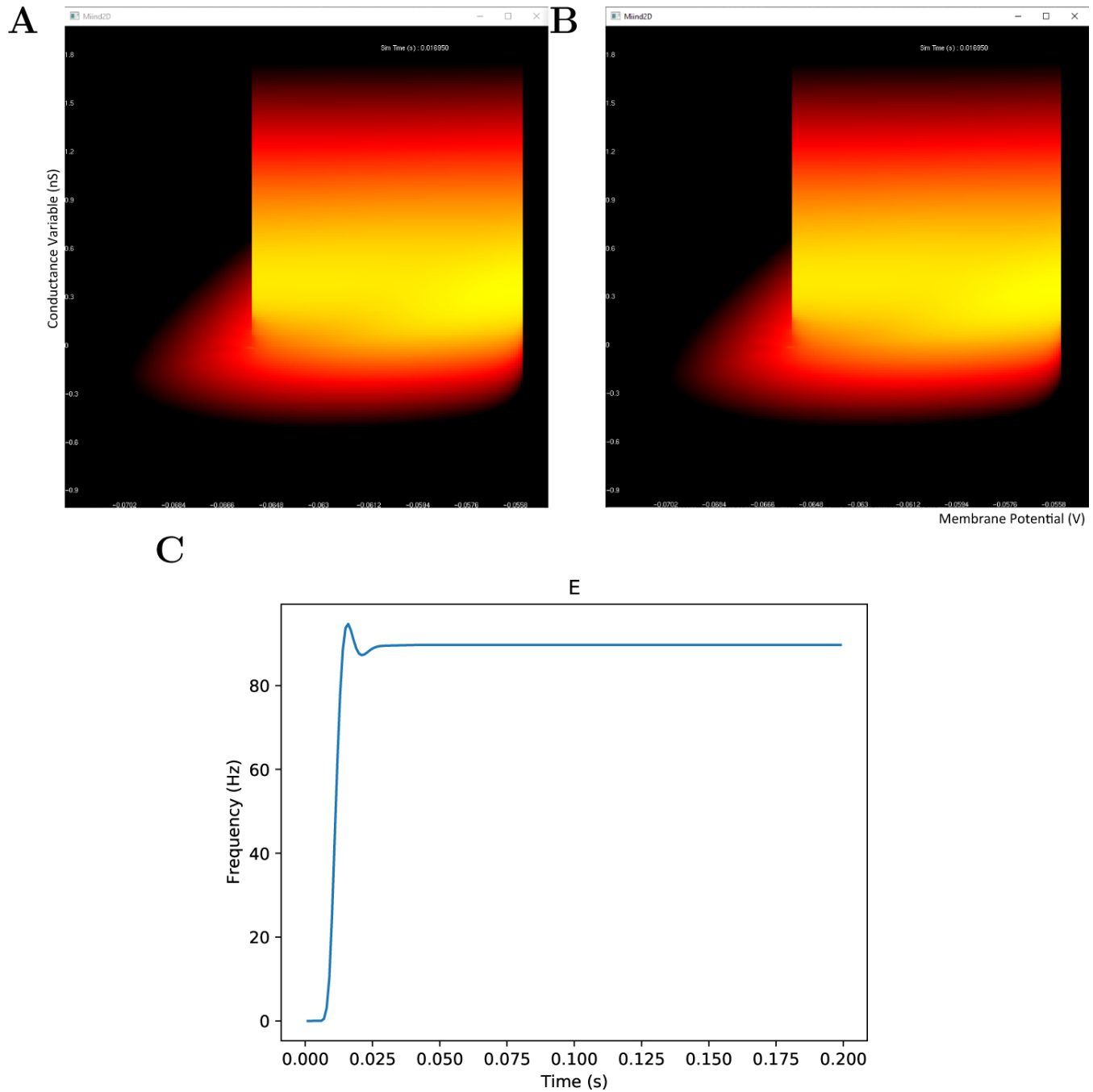


Figure 2. The display output of a running E-I population network simulation of conductance based neurons. (A) The probability density heat map of the excitatory population. (B) The probability density heat map of the inhibitory population. Brighter colours indicate a larger probability mass. The axes are unlabelled in the simulation windows as the software is agnostic to the underlying model. However, the membrane potential and conductance labels have been added for clarity. (C) The average firing rate of the excitatory population.

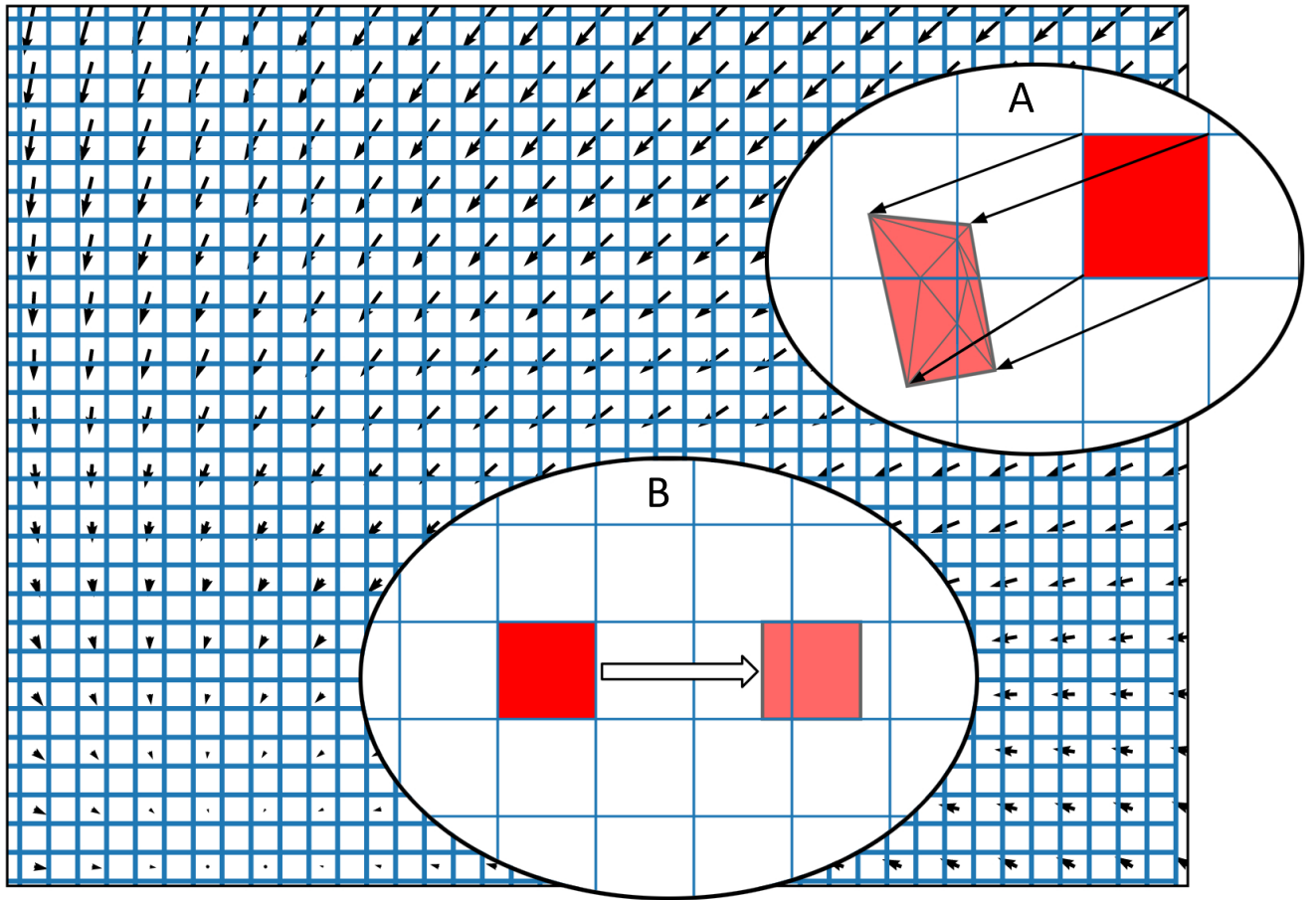


Figure 3. The state space of a neuron model (shown here as a vector field) is discretised into a regular grid of cells. (A) The transition matrix for solving the deterministic dynamics of the population is generated by applying a single time step of the underlying neuron model to each vertex of each cell in the grid and calculating the proportion by area to each overlapping cell. Once the vertices of a grid cell have been translated, the resulting polygon is recursively triangulated according to intersections with the original grid. Once complete, all triangles can be assigned to a cell and the area proportions can be summed. (B) For a single incoming spike (with constant efficacy), all cells are translated by the same amount and therefore have the same resulting transition which can be used to solve the Poisson master equation. In fact, the transition will always involve at most two target cells and the proportions can be calculated knowing only the grid cell width and the efficacy.

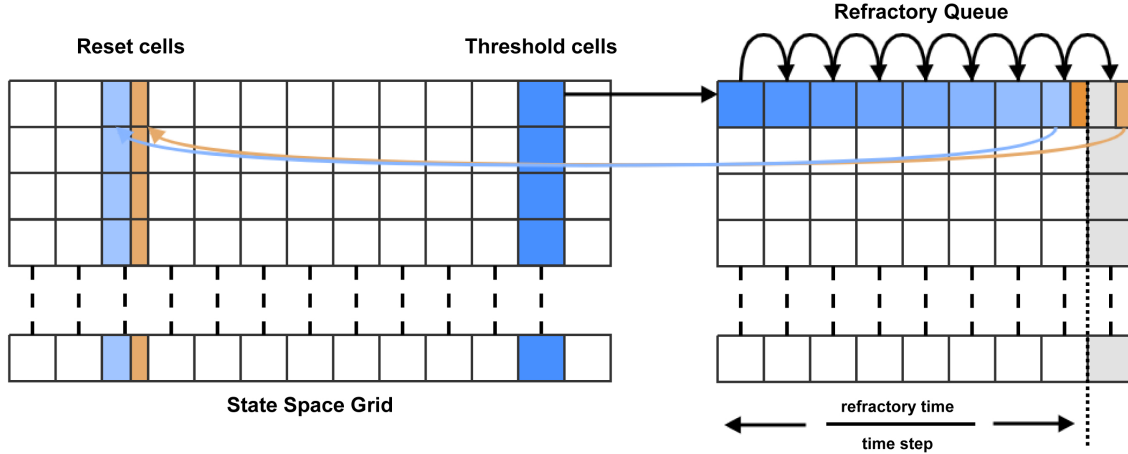


Figure 4. For each time step, probability mass in the cells which lie across the threshold (threshold cells) is pushed onto the beginning of the refractory queue. There is one queue per threshold cell. During each subsequent time step, the probability mass is shifted one place along the queue until it reaches the penultimate place. A proportion of the mass, calculated according to the modulo of the refractory time and the time step, is transferred to the appropriate reset cell. The remaining mass is shifted to the final place in the queue. During the next time step, that remaining mass is transferred to the reset cell.

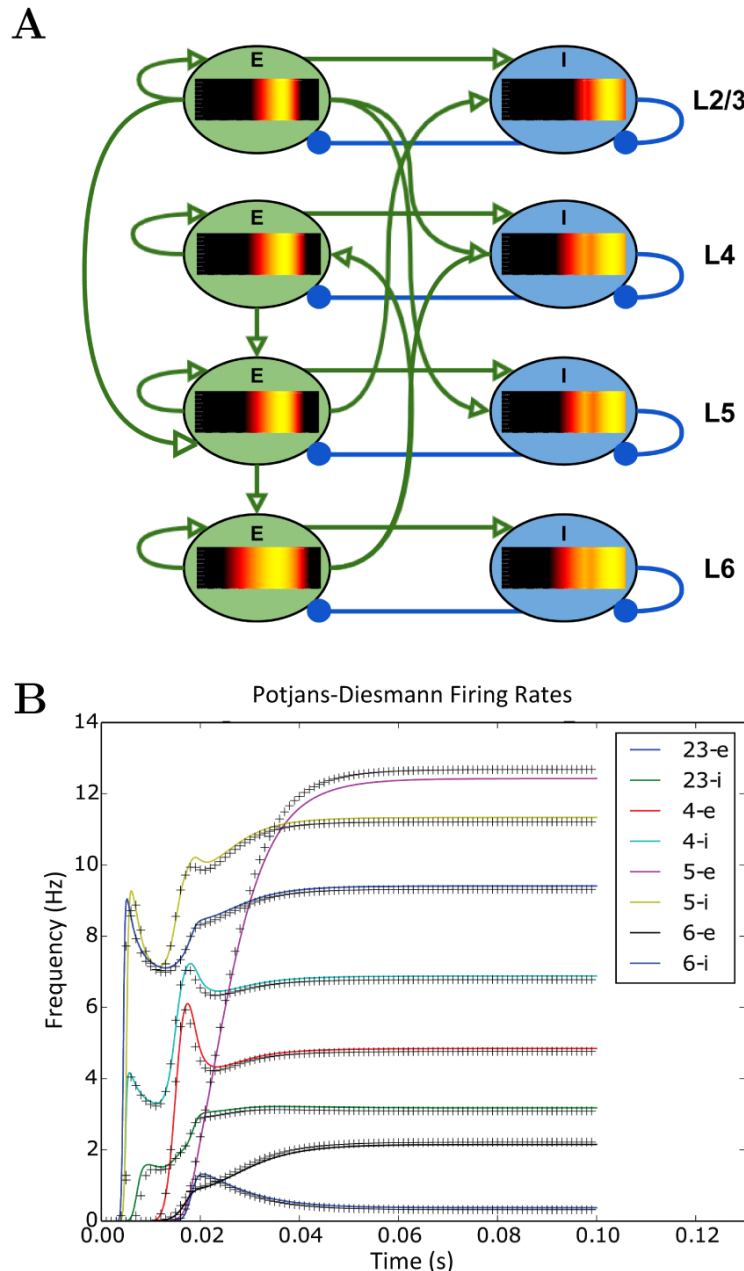


Figure 5. (A) A representation of the connectivity between populations in the Potjans-Diesmann microcircuit model. Each population shows the probability density at an early point in the simulation before all populations have reached a steady state. All populations are of leaky-integrate-and-fire neurons and so the density plots show membrane potential in the horizontal axis. The vertical axis has no meaning (probability mass values are the same at all points along the vertical). (B) The firing rate outputs from MIIND (crosses) in comparison to those from DiPDE for the same model (solid lines).

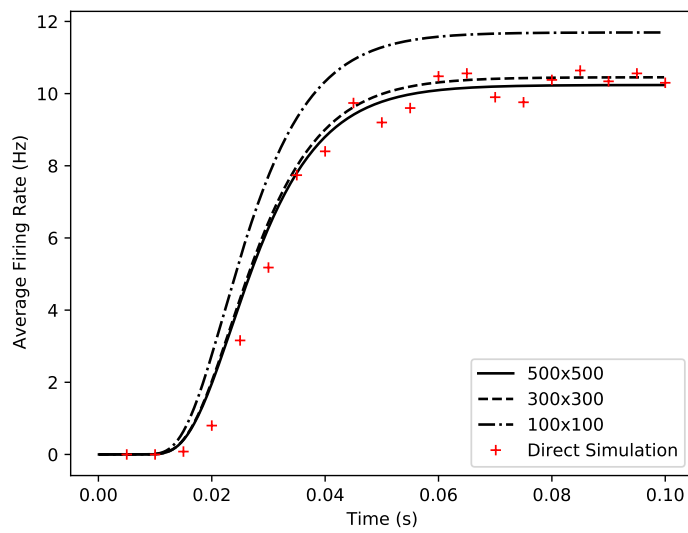


Figure 6. Comparison of average firing rates from four simulations of a single population of conductance based neurons. The black solid and dashed lines indicate MIIND simulations using the grid algorithm with different grid resolutions. The red crosses show the average firing rate of a direct simulation of 10,000 neurons.

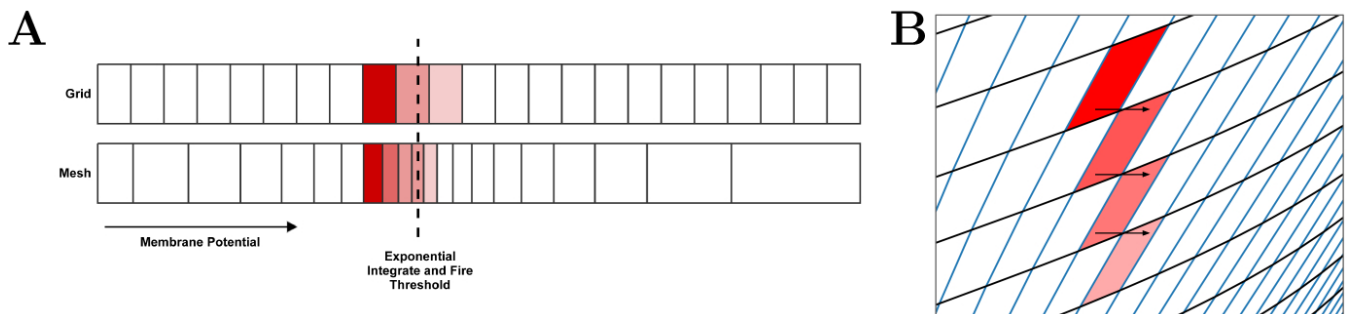


Figure 7. (A) In the grid algorithm, large cells cause probability mass to be distributed further than it should. This error is expressed most clearly in models where the the average firing rate of the population is highly dependent on the amount of probability mass passing through an area of slow dynamics. (B) In the mesh algorithm, when cells become shear, probability mass which is pushed to the right due to incoming spikes also moves laterally (downwards) because it is spread evenly across each cell.

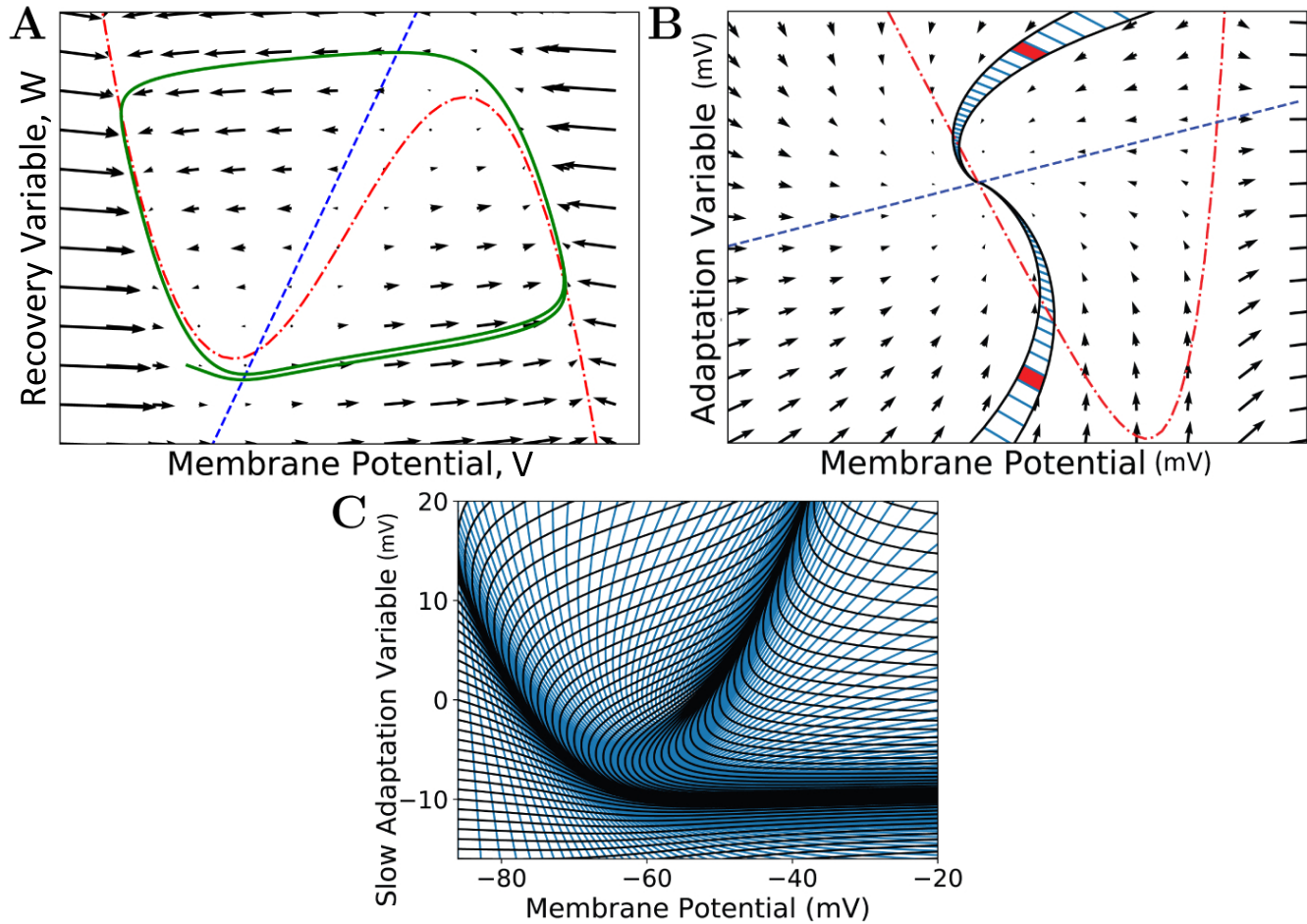


Figure 8. (A) A vector field of the FitzHugh-Nagumo neuron model (FitzHugh, 1961). Arrows show the direction of motion of states through the field according to the dynamics of the model. The red broken dashed nullcline indicates where the change in V is zero. The blue dashed nullcline indicates where the change in W is zero. The green solid line shows a potential path (trajectory) of a neuron in the state space. (B) A vector field for the adaptive exponential integrate and fire neuron model (Brette and Gerstner, 2005). Two strips are shown which follow the dynamics of the model and approach the stationary point where the nullclines cross. A strip is constructed between two trajectories in state space. Each time step of the two trajectories is used to segment the strip into cells. Because the strips approach a stationary point, they get thinner as the trajectories converge to the same point and cells get closer together as the distance in state space travelled reduces per time step (neurons slow down as they approach a stationary point). Per time step, probability mass is shifted from one cell to the next along the strip. (C) The state space of the Izhikevich simple neuron model (Izhikevich, 2003) which has been fully discretised into strips and cells.

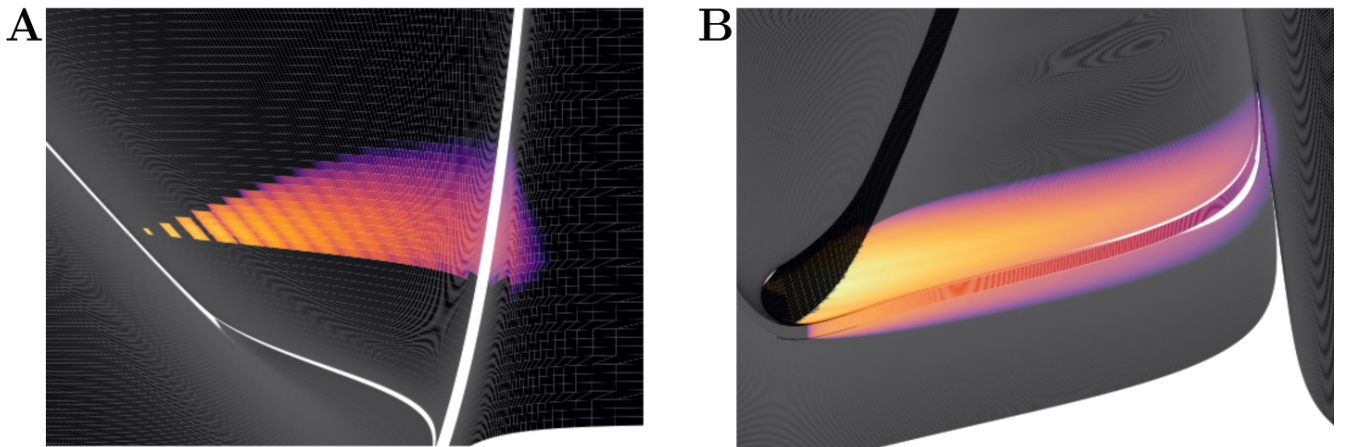


Figure 9. Heat plots for the probability density functions of two populations in MIIND. Brightness (more yellow) indicates a higher probability mass. (A) When the Poisson master equation is solved, probability mass is pushed to the right (higher membrane potential) in discrete steps. As time passes, the discrete steps are smoothed out due to the movement of mass according to the deterministic dynamics (following the strip). (B) A combination of mass travelling along strips and being spread across the state space by noisy input produces the behaviour of the population.

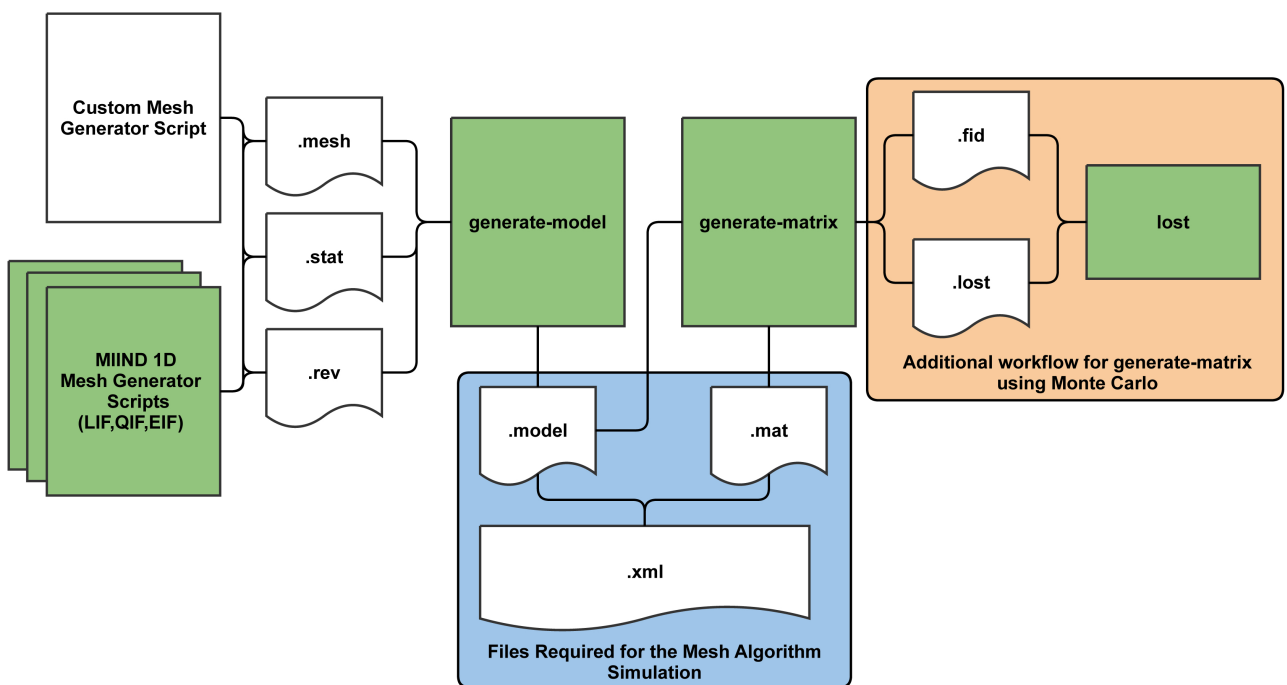


Figure 10. The MIIND processes and generated files required at each stage of pre-processing for the mesh algorithm. The shaded green rectangles represent automated processes run via the MIIND CLI.

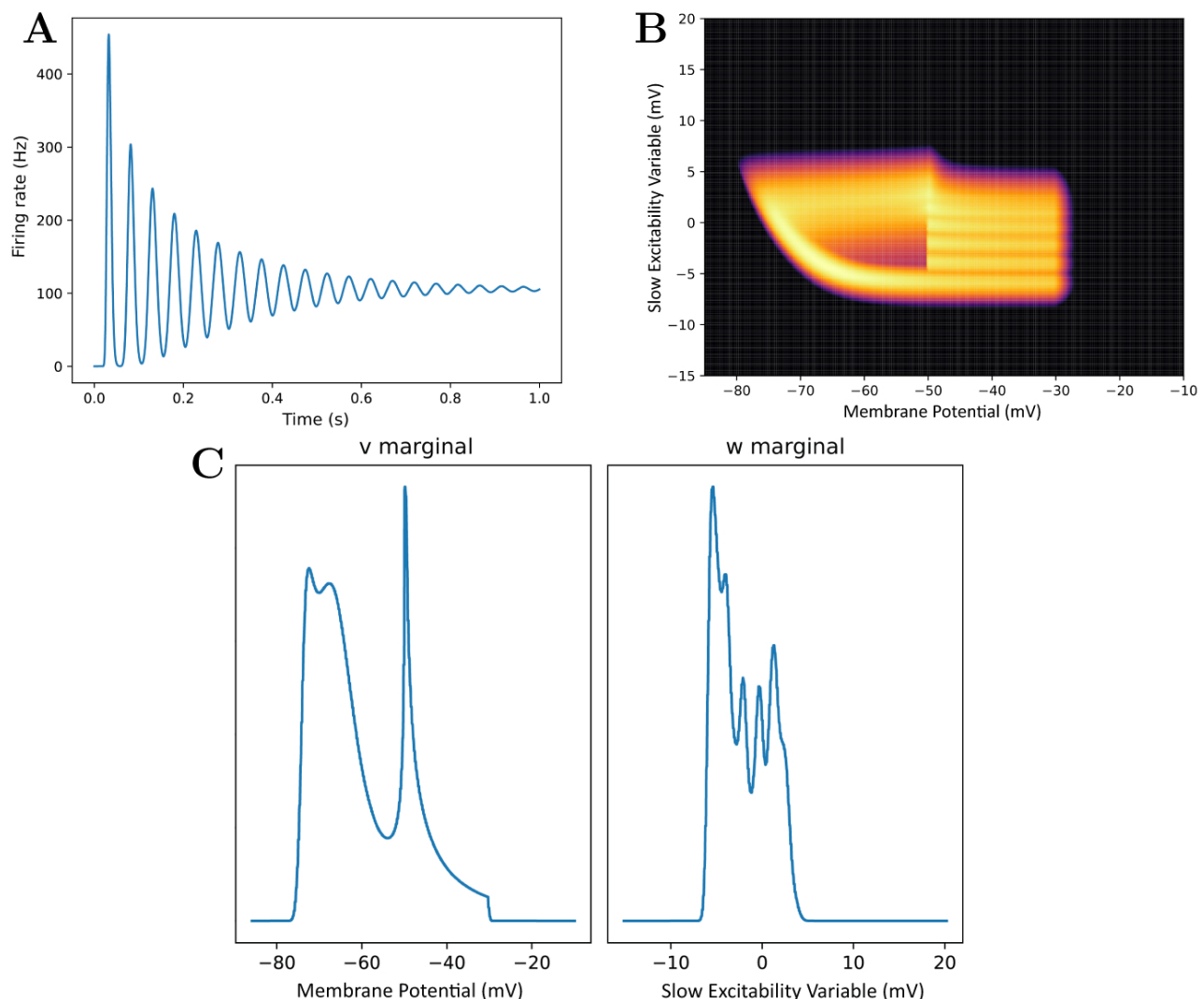


Figure 11. (A) The average firing rate of a population produced by calling the **rate** command. (B) A density plot of the population produced by calling the **plot-density** command. (C) The marginal density plots produced by calling the **plot-marginals** command.

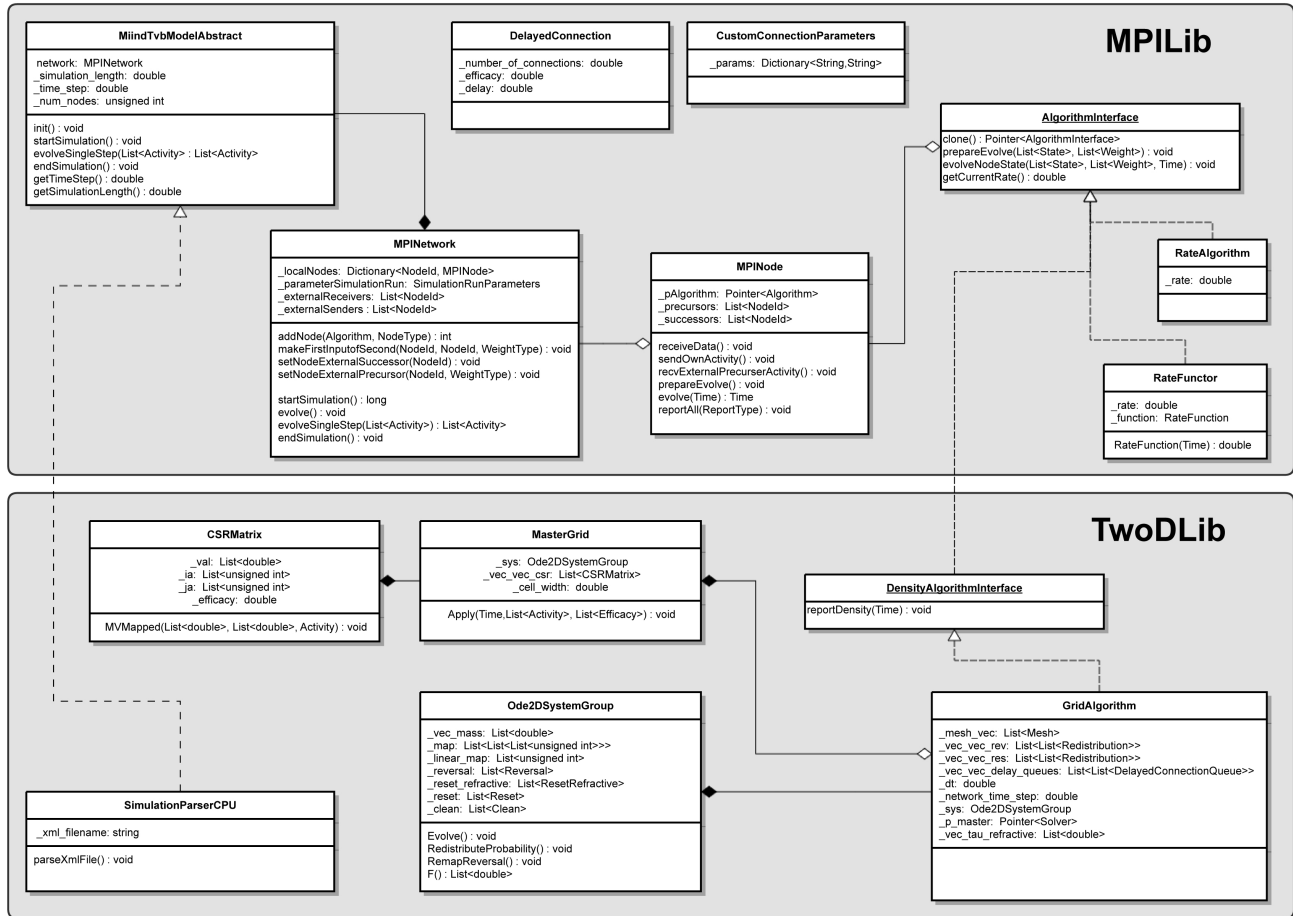


Figure 12. A minimal UML diagram of MIIND. The two major libraries, MPILib and TwoDLib, are represented.

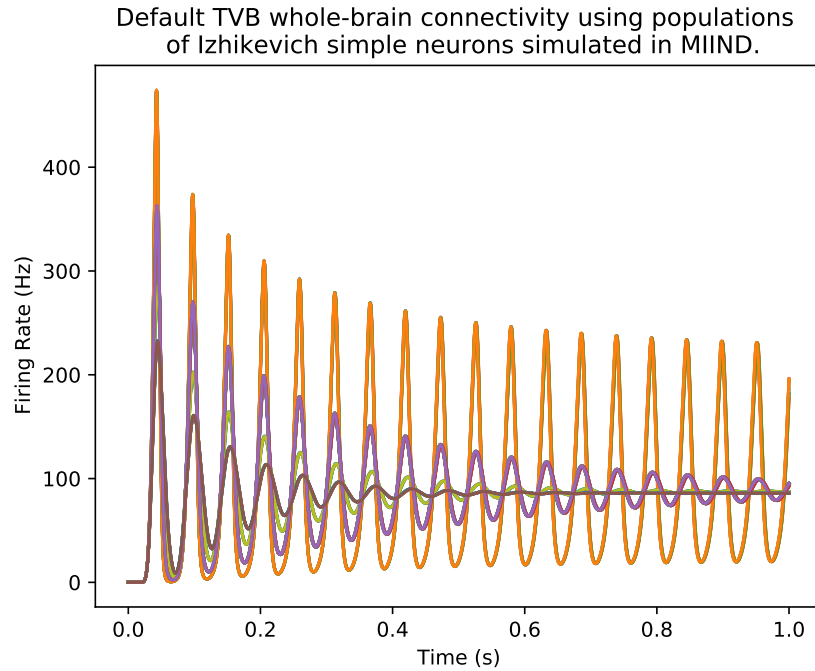


Figure 13. The firing rates of 76 nodes from the default TVB connectivity simulation. Each node is a population of Izhikevich simple neurons simulated using MIIND. The majority of nodes produce oscillations which decay to a constant average firing rate. However, a subset of nodes remain in an oscillating state.

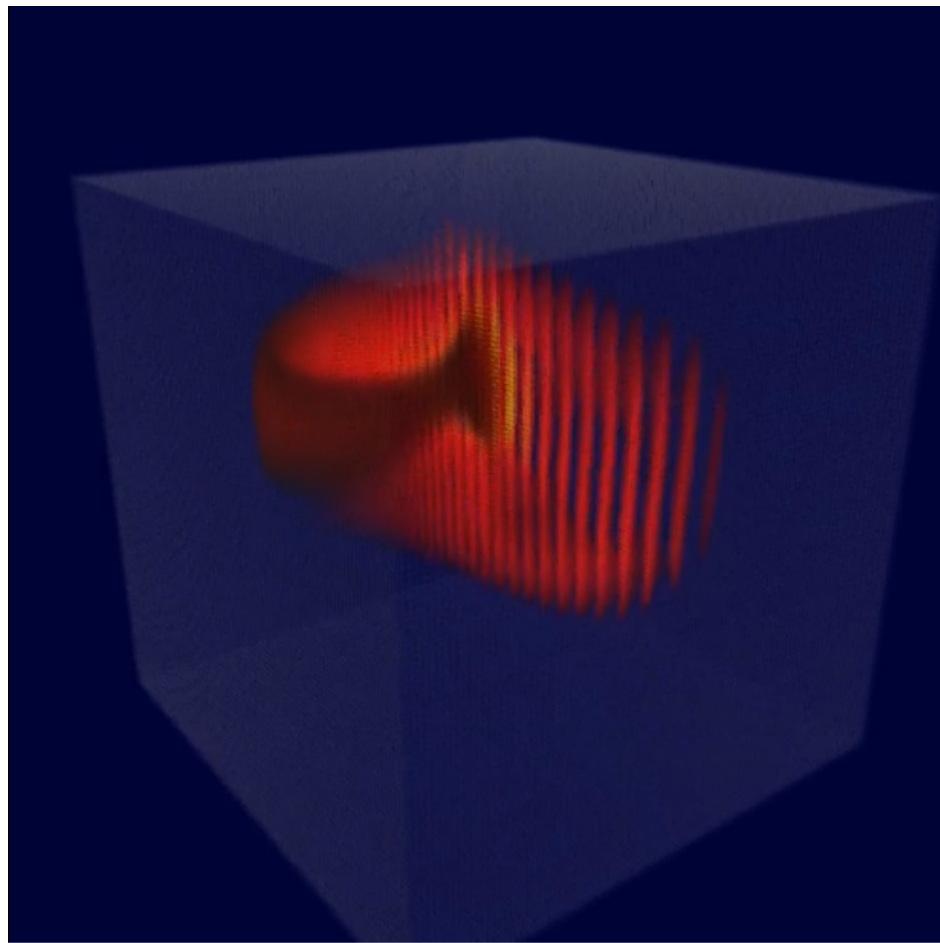


Figure 14. (A) A density plot of a population of Hindmarsh-Rose neurons. The density is contained in a three dimensional volume such that each axis represents one of the time-dependent variables of the model. The volume has been rendered from a rotated and elevated position to more easily visualise the density.